



National Library
of Canada

Bibliothèque nationale
du Canada

Canadian Theses Service

Service des thèses canadiennes

Ottawa, Canada
K1A 0N4

NOTICE

The quality of this microform is heavily dependent upon the quality of the original thesis submitted for microfilming. Every effort has been made to ensure the highest quality of reproduction possible.

If pages are missing, contact the university which granted the degree.

Some pages may have indistinct print especially if the original pages were typed with a poor typewriter ribbon or if the university sent us an inferior photocopy.

Previously copyrighted materials (journal articles, published tests, etc.) are not filmed.

Reproduction in full or in part of this microform is governed by the Canadian Copyright Act, R.S.C., 1970, c. C-30.

AVIS

La qualité de cette microfôrme dépend grandement de la qualité de la thèse soumise au microfilmage. Nous avons tout fait pour assurer une qualité supérieure de reproduction.

S'il manque des pages, veuillez communiquer avec l'université qui a conféré le grade.

La qualité d'impression de certaines pages peut laisser à désirer, surtout si les pages originales ont été dactylographiées à l'aide d'un ruban usé ou si l'université nous a fait parvenir une photocopie de qualité inférieure.

Les documents qui font déjà l'objet d'un droit d'auteur (articles de revue, tests publiés, etc.) ne sont pas microfilmés.

La reproduction, même partielle, de cette microfôrme est soumise à la Loi canadienne sur le droit d'auteur, SRC 1970, c. C-30.

THE UNIVERSITY OF ALBERTA

A Nonlinear Finite Element Study of A Lumbar
Intervertebral Motion Segment

BY

Fan Zhang

A THESIS

SUBMITTED TO THE FACULTY OF GRADUATE STUDIES AND RESEARCH IN PARTIAL
FULFILMENT OF THE REQUIREMENTS FOR THE DEGREE OF MASTER OF SCIENCE.

DEPARTMENT OF MECHANICAL ENGINEERING

EDMONTON, ALBERTA

FALL 1987

Permission has been granted to the National Library of Canada to microfilm this thesis and to lend or sell copies of the film.

The author (copyright owner) has reserved other publication rights, and neither the thesis, nor extensive extracts from it may be printed or otherwise reproduced without his/her written permission.

L'autorisation a été accordée à la Bibliothèque nationale du Canada de microfilmer cette thèse et de prêter ou de vendre des exemplaires du film.

L'auteur (titulaire du droit d'auteur) se réserve les autres droits de publication; ni la thèse ni de longs extraits de celle-ci ne doivent être imprimés ou autrement reproduits sans son autorisation écrite.

ISBN 0-315-40938-X

THE UNIVERSITY OF ALBERTA

RELEASE FORM

NAME OF AUTHOR: Fan Zhang

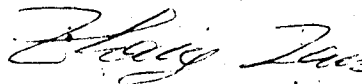
TITLE OF THESIS: A Nonlinear Finite Element Study of A Lumbar
Intervertebral Motion Segment

DEGREE: Master of Science

YEAR THIS DEGREE GRANTED: 1987

Permission is hereby granted to THE UNIVERSITY OF ALBERTA LIBRARY to reproduce single copies of this thesis and to lend or sell such copies for private, scholarly or scientific research purposes only.

The author reserves other publication rights, and neither the thesis nor extensive extracts from it may be printed or otherwise reproduced without the author's written permission.



(Student's signature)

Date: August 6th, 1987

THE UNIVERSITY OF ALBERTA
FACULTY OF GRADUATE STUDIES AND RESEARCH

The undersigned certify that they have read, and recommend to the Faculty of Graduate Studies and Research for acceptance, a thesis entitled A Nonlinear Finite Element Study of A Lumbar Intervertebral Motion Segment submitted by Fan Zhang in partial fulfilment of the requirements for the degree of Master of Science.


(Supervisor)





Date: August 6th, 1987

Dedicated to my parents.

ABSTRACT

Many of the problems associated with the human spine are partly structural in nature. Scoliosis, for example, involves a significant deformation of the spine due to instability. Internal fixation is employed in the management of spinal fractures. To assist in the understanding of these structural problems, detailed modeling of spine mechanics is essential.

This study intends to serve as a first stage of modeling spine fixation systems by investigating fundamental behaviour of a disc-body unit.

A three-dimensional finite element packaged program ADINA (fluid-structure compatible) is used including both geometric and material nonlinearities. Five hundred and twelve elements, eighteen hundred and nine degrees of freedom, are employed in this study.

Validation of the model by a comparison of its predictions with reported results of "in vitro" measurements indicates good agreement. Intradiscal boundary conditions are verified through investigating stress distribution on the end-plate and end-plate deflections. Further sophistication of the model to capture important characteristics of the spine behaviour is suggested. This includes simplification of some of the non-critical components in order to simplify calculations.

ACKNOWLEDGEMENT

The author would like to thank his supervisor, Professor D. Budney, for his advice and constant encouragement through this study.

The author is grateful to J. Raso, Director of the Biomechanics Laboratory at the Glenrose Hospital for his valuable suggestions.

This study was supported through Medical Research Council, Grant No. 55-42430. The author also wishes to express his thanks to Dr. M. Moreau.

Special thanks are extended to Mr. F. Wright for discussion and Mr. T. Kaiser for his assistance in computer programming.

CONTENTS

Chapter 1: Introduction

1-1: Function of the spine	1
1-2: Anatomy of the human spine	4
1-3: The basic unit of the spine system: the motion segment	6
1-4: Relevant anatomy of a motion segment	9
1-5: Kinematics of the spine	13
1-6: Loads on a motion segment	15
1-7: Importance of spinal biomechanics	16
1-8: Challenges of modeling spine fixation systems	17
1-9: Objectives of this study	18

Chapter 2: Numerical model for the lumbar

intervertebral body-disc-body unit

2-1: Review of previous work	19
2-2: Technical aspects of modeling the intervertebral disc	23
2-3: A fluid-structure compatible formulation	25
2-4: Some aspects concerning material and geometric properties	35
2-5: Loading and boundary conditions	39

Chapter 3: Numerical results

3-1: Validation of the present F.E. model	46
3-2: Stress distribution on the end-plate	49
3-3: End-plate deformation	55
3-4: Collagenous fiber strain and disc bulging related to clinical symptoms	58
3-5: Gross disc behaviour under separate loads	62

Chapter 4: Modeling the annulus fibrosus

4-1: Introduction	64
4-2: Stresses in the end-plate in two different models	66
4-3: Modeling sliding between the collagenous fibers and the ground substances	68
4-4: Modeling the annulus fibrosus	70

Chapter 5: Discussion and conclusion

5-1: Material properties	72
5-2: Stresses on the end-plate and end-plate bulging	73
5-3: Limitations of this study	75
5-4: Conclusions	76

References	79
------------	----

Appendix A: Introduction of ADINA	87
-----------------------------------	----

LIST OF TABLES

Table 2.3-1: Finite element matrices for Updated Lagrangian formulation	33
Table 2.4-1: Overall dimensions of the lumbar vertebral model	35
Table 2.4-2: Distribution of collagenous fibres among layers	36
Table 2.4-3: Material properties of the bony parts and the annulus	38

LIST OF FIGURES

Fig. 1.1-1: Typical vertebrate - dinosaur	2
Fig. 1.1-2: The human skeleton	3
Fig. 1.2-1: Lateral view of the human vertebral column	5
Fig. 1.3-1: Function unit of the spine - The motion segment	7
Fig. 1.3-2: The lumbar vertebra, side view	8
Fig. 1.3-3: The lumbar vertebra, from above	8
Fig. 1.4-1: The intervertebral disc	10
Fig. 1.4-2: Sectional view of the cartilaginous end-plate	10
Fig. 1.5-1: Coordinate system defined	14
Fig. 2.3-1: Motion of body in stationary, Cartesian coordinate system	26
Fig. 2.4-1: Constitutive curve for the collagenous fiber	37
Fig. 2.5-1: Outline of the present finite element model	41
Fig. 2.5-2: Posterolateral view of the present model (Under axial torsion)	42
Fig. 2.5-3: Posterolateral view of the present model (Under flexion)	43
Fig. 2.5-4: Posterolateral view of the present model (Under extension)	44

Fig. 2.5-5: Posterolateral view of the present model (Under right lateral bending)	45
Fig. 3.1-1: Disc behaviour under compression	48
Fig. 3.1-2: Intradiscal pressure under compression	48
Fig. 3.2-1: Normal stress σ_{zz} distribution on the end-plate (Under compression)	50
Fig. 3.2-2: Shear stress σ_{zx} distribution on the end-plate (Under compression)	52
Fig. 3.2-3: Normal stress σ_{zz} distribution on the end-plate (Under flexion)	52
Fig. 3.2-4: Normal stress σ_{zz} distribution on the end-plate (Under extension)	53
Fig. 3.2-5: Normal stress σ_{zz} distribution on the end-plate (Under right lateral bending)	53
Fig. 3.2-6: Shear stress σ_{zy} distribution on the end-plate (Under axial torsion)	54
Fig. 3.3-1: End-plate bulging	56
Fig. 3.3-2: Nondimensional end-plate bulging parameter	56
Fig. 3.3-3: End-plate deformation under compression, extension and flexion	57
Fig. 3.4-1: Posterior relationship of the lumbar nerve root	59
Fig. 3.4-2: A sequestered disc may compress the nerve root	59
Fig. 3.4-3: Posterior collagenous fiber strain	60

Fig. 3.4-4: Posterolateral collagenous fiber strain	60
Fig. 3.4-5: Horizontal disc bulging	61
Fig. 3.5-1: Disc sagittal plane rotation	63
Fig. 4.2-1: Normal stress σ_{zz} distribution	
(With two different models)	67
Fig. 4.2-2: Shear stress σ_{zy} distribution	
(With two different models)	67
Fig. 4.3-1: Collagenous fiber elements and	
ground substance element fixed together	69
Fig. 4.3-2: Two kinds of element allowed to slide on each other	69

CHAPTER 1: INTRODUCTION

1-1: FUNCTION OF THE SPINE

An axial endoskeletal structure, the vertebral column, is one of the major distinguishing characteristics of vertebrates (Fig. 1. 1-1). As the most advanced vertebrate, the human has a body structure (Fig. 1.1-2), including the vertebral column, which is the result of 500 million years of evolution.

The spine is a mechanical structure. The vertebrae articulate with each other in a controlled manner through a complex system of joints, discs, ligaments and soft tissues. In the thoracic region, the spine is markedly stiffened by the rib cage. Although the spine has some inherent ligament stability, mechanical stability is maintained primarily by a highly developed, dynamic neuromuscular structure and its control system.

The spine performs at least three fundamental biomechanical functions. First, it transfers the weight and the bending moment of the head and trunk to the pelvis. Second, it allows physiological motion between these three body parts. Finally and most importantly, it protects the delicate spinal cord from potentially damaging forces or motions produced by trauma. These functions are accomplished through the highly specialized mechanical properties of the normal spine anatomy.

Page 2 has been removed due to copyright restriction. This page
contained:

TYPICAL VERTEBRATE - DINOSAUR

(From McFarland et al., 1979)

Page 3 has been removed due to copyright restriction. This page
contained:

THE HUMAN SKELETON (FRONTAL VIEW)

(From Cairney J. and Cairney John, 1974)

1-2: ANATOMY OF THE HUMAN SPINE

The spine consists of seven cervical (neck) vertebrae, twelve thoracic (chest) vertebrae, five lumbar (low back) vertebrae, and three to four fused coccygeal segments. Viewed from the front, the spine generally appears straight and symmetrical. In the lateral or sagittal plane there are four normal curves. These curves are convex anteriorly in the cervical and lumbar regions and convex posteriorly in the thoracic and sacral regions (Fig.1.2-1).

Anatomical considerations relating the whole spine are important, but it is also necessary to observe, study, and consider the regional characteristics of the spine. The lumbar region is unique in that it is most likely to be injured due to the fact that the lumbar segment, unlike the thoracic segment, is not supported by the rib cage. Therefore, it supports very high loads.

Page 5 has been removed due to copyright restriction. This page
contain: LATERAL VIEW OF THE HUMAN VERTEBRAL COLUMN
(From White and Panjabi, 1978)

1-3: THE BASIC UNIT OF THE SPINE SYSTEM: THE MOTION SEGMENT

The functional unit of the spine is the motion segment, which consists of two vertebrae, the articular joint, the intervertebral disc and seven ligaments (Fig. 1.3-1). A vertebra consists of an anterior block of bone, the body, and a posterior bony ring, known as the neural arch, containing articular, transverse, and spinous processes (Fig. 1.3-2, 1.3-3). The neural arch consists of two pedicles and two laminae from which arise seven processes. The arches and the vertebral bodies form the vertebral canal, which protects the spinal cord.

Page 7 has been removed due to copyright restriction. This page
contained: FUNCTIONAL UNIT OF THE SPINE - THE MOTION SEGMENT

(From White and Panjabi, 1978)

Page 8 has been removed due to copyright restriction. This page
contained:

THE LUMBAR VERTEBRA, SIDE VIEW

(From Grant, 1972)

and

THE LUMBAR VERTEBRAL, FROM ABOVE

(From Grant, 1972)

1-4: THE RELEVANT ANATOMY OF A MOTION SEGMENT

The intervertebral disc is comprised of three distinct parts: the nucleus pulposus, the annulus fibrosus, and the cartilaginous end-plate (Fig. 1.4-1).

The nucleus pulposus is a centrally located region composed of a very loose and transparent network of fine fibres that lie in a mucoprotein gel containing various mucopolysaccharides. The fine collagen fibres play a part in stabilization of the gel. The fluid is primarily immobilized by the mucopolysaccharides. The water content ranges from 70 to 90 percent; it is highest at birth and tends to decrease with age. The lumbar nucleus fills 30 to 50 percent of the total disc cross-sectional area. In the lumbar region, the nucleus is located more posteriorly. It is believed that the nucleus is readily deformable because of its jelly-like nature and can transmit applied load to a thrust on the annulus (Nachemson, 1960). It is, therefore, important for optimal function of the disc that the nucleus remains fluid.

The annulus fibrosus is the outer region of the intervertebral disc. There is a gradual transition of material structure from the nucleus to the annulus, and through the annulus itself. The distinction between annulus and nucleus, although pronounced, is not sharply defined, but a gradual change does occur from the jelly-like nucleus to the more fibrous annulus. The annulus is composed of fibrous tissue in concentric laminated bands. The collagen fibres provide strength and

Page 10 has been removed due to copyright restriction. This page
contained: THE INTERVERTEBRAL DISC

(Cartilaginous end, plate is not shown, from White and Panjabi, 1978)
and

SECTIONAL VIEW OF THE CARTILAGINOUS END-PLATE

(From Cairney J. and Cairney John, 1974)

stiffness to the annulus tissue. The ground substance, a gelatinous material, reduces friction between the collagen fibres (Frankel and Nordin, 1980). The collagen fibres are arranged in a helicoid manner so that in a given band the fibres have a relatively constant direction. The fibres in an adjacent band are aligned in the opposite direction. They are oriented at 30 degrees to the disc plane and therefore at 120 degrees to each other in adjacent bands. The laminated structure is uniquely adapted to provide both mobility and an ability to withstand the tensile strain that occur from compression, bending and rotation. With increasing compressive load, bulging of the annulus causes the layers to tighten and bind together so that tension in the collagen fiber withstands pressure developed in the nucleus pulposus.

The cartilaginous end-plate is composed of hyaline cartilage. It separates the other two components of the disc from the vertebral body (Fig. 1.4-2). Physiologically, cartilage is virtually an isolated tissue. It is devoid of blood and lymphatic supplies as well as nerves, and its cellular density is less than in most other tissues. The main functions of cartilage are to distribute the loads applied to the joint so that they are transmitted over a large area and thus reduce contact stresses and to allow relative movement of the opposing surfaces with minimum friction and wear.

The vertebral body is a roughly cylindrical mass of cancellous bone contained in a thin shell of cortical bone (Fig. 1.3-3). These two bone types can be considered as one material whose porosity varies over a wide range (Carter and Hayes 1977). (Porosity is the proportion of the

bone's volume occupied by nonmineralized (non bone) tissues). Cortical bone is stiffer than cancellous bone; it can withstand greater stress but less strain before failure. Cortical bone fractures "in vitro" when the strain exceeds 2% of the original length; cancellous bone does not fracture until the strain exceeds 7%. Because of its porous structure, cancellous bone has been shown to have a high energy storage capacity (Carter and Hayes, 1976). Both cortical bone and cancellous bone are anisotropic materials (material properties are different in all directions at a point in the body). The strength and stiffness are greatest in the direction in which loads are most commonly imposed on the bone (Cowin, 1983).

1-5: KINEMATICS OF THE SPINE

The coordinate system employed in this study is defined as Fig. 1.5-1. The right-handed orthogonal, or Cartesian coordinate system is defined for precise orientation with respect to the body: In Fig. 1.5-1, the human body is shown in the anatomic position (upright position with the eyes and toes directed forward and the arms hanging at the sides, with the palms forward). The sagittal, frontal and horizontal planes are represented by x-z, y-z and x-y planes respectively. Motion is described in terms relative to the inferior (the lower) vertebra.

During physiological activities, motion can be described as rotation, translation, or a combination of them. The clinical nomenclature of spine movement in the defined coordinate system is (Fig. 1.5-1):

Flexion:	clockwise rotation about Y-axis.
Extension:	anticlockwise rotation about the Y-axis.
Axial rotation:	rotation about Z-axis.
Lateral bending:	rotation about X-axis.
Axial compression:	translation in negative Z-axis direction.

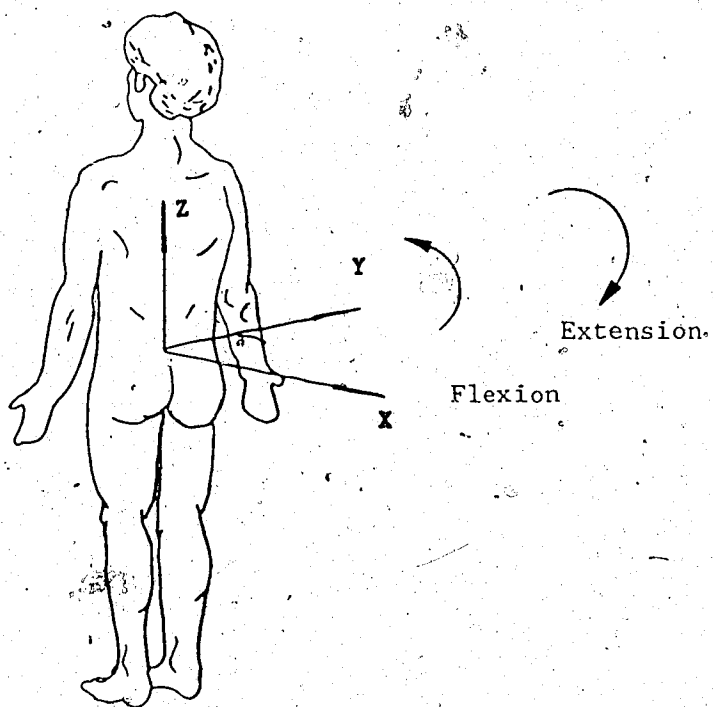


Figure 1-5-1: COORDINATE SYSTEM DEFINED
(Human figure in anatomic position)

1-6: LOADS ON THE MOTION SEGMENT

The intervertebral disc is subjected to a considerable variety of forces and moments. It is responsible for carrying a large part of the compressive loads applied to the trunk (Nachemson, 1960). When a person is standing in the anatomic position, muscular activity causes greater force on a disc than the superior weight of the body. In addition, with any activity where dynamic loads are involved (e.g. jumping or trauma) the actual loads on the intervertebral disc are much higher than the static load. These are mainly compressive loads, producing compressive stresses in the disc. The disc is also subjected to other types of loads and stresses. Tensile stresses are produced in certain portions of the disc during physiologic motions of compression, flexion, extension, and lateral bending. Axial rotation of the torso with respect to the pelvis causes torsional loads which result in shear stresses in the disc. Due to the laminated asymmetric structure of the annulus fibrosus, rotation and bending are known to be coupled. This results in a combination of tensile, compressive, and shear stresses in the disc (Ueno and Liu, 1985; Shirazi-Adl et al, 1986).

The loads can be divided into two main categories according to the time duration of application. There are short duration loads of high amplitude (e.g. jerk lifting) and long duration, low magnitude loads due to more normal physical activity. This division is important, since the disc exhibits certain time-dependent behaviour such as fatigue and viscoelasticity which can be characterized by creep and relaxation.

1-7: IMPORTANCE OF SPINAL BIOMECHANICS

Internal fixation is employed increasingly in the management of spinal fractures. Posterior stabilization techniques based on the use of Harrington-compression rods, Harrington-distraction rods and Luque segmental instrumentation etc. are frequently used. In the thoracolumbar spine, posterior stabilization has usually involved fixation from as many as three vertebrae above to two or three below the damaged level.

Investigations have been carried out to test and compare the effectiveness of various possible posterior techniques in resisting different kinds of loads. There are two ways of examining the available spinal surgery devices, namely experimental and analytical methods.

For experimental work, the use of cadaver spines seems the most obvious choice but has the inherent disadvantages of large variation in age, size and strength. Although experimental work has been done to measure the intradiscal pressure, end-plate and disc bulging, surface strain of the disc and the vertebra etc., little has been done using cadaver spine to evaluate the effectiveness of the different fixation devices' (McAfee et al, 1985). An appropriate "in vitro" animal model providing qualitative values for fixation in the human spine may be suitable for the comparison of techniques. An analytical model, if done properly can provide a direct and less expensive way to demonstrate the effectiveness of available fixation devices. Furthermore, it can serve as a measure to design new instruments. The analytical model can also be used to describe the behaviour of an uninjured spinal column, which is important reference information for the study of a instrumented spine.

1-8: CHALLENGES OF MODELING THE SPINE FIXATION SYSTEMS

The successful modeling of the spine-fixation device system depends on four main aspects:

- (1) modeling the human spine, especially the intervertebral disc behaviour;
- (2) modeling the intradiscal boundary conditions;
- (3) modeling the articular facet boundary conditions; and
- (4) modeling of the interaction between spine model and fixation devices.

1.9: OBJECTIVES OF THIS STUDY

The present study intends to serve as a first stage of modelling the spine fixation systems by investigating the fundamental behaviour of a motion segment under different loading conditions. It is expected that, as a result of this work, the boundary conditions and the contributions of the disc to the whole spinal column, can be verified. Further sophistication of the model to capture the important characteristics of the spine behaviour, can be suggested after this study.

CHAPTER 2: NUMERICAL MODEL FOR THE LUMBAR

INTERVERTEBRAL BODY-DISC-BODY UNIT

2-1: REVIEW OF PREVIOUS WORK

Mathematical models of the disc have been constructed to provide behavioral details which are not easily measured. Some disc models provide complete displacement, stress, and strain distributions to evaluate gross disc behaviour, annular tearing, end-plate fracture, and subsequent material remodeling. Disc models also lead readily to parameter studies, so that the influences of geometry and material property variations on disc behaviour can be gauged; i.e., to identify those parameters which are significant determinants of disc response. Disc models can incorporate various degrees of sophistication.

Two primary categories of the intervertebral disc models which have appeared in the literatures are analytical models and numerical models. In general, the analytical models attempt to establish simple analytic relations between the fundamental parameters of the disc model, such as pressure in the nucleus versus applied compressive pressure, bulging versus change in disc height, etc.. Early models were developed by Nachemson(1960) and Sonnersup(1972). These models assumed that the nucleus and the annulus form two concentric circular cylinders. The stress distribution in the annulus was studied using this model. More

recently, Hickey and Hukins(1980) constructed a simple semianalytic model which identifies fiber involvement in layers of incompressible fluid in the annulus. They compared response under compression and torsional loading with results obtained experimentally. Broberg and Von Esson(1980) also included fibres (with nonlinear force-elongation relations) imbedded in compartments (layers) of incompressible fluid. They compared model responses under compressive loading with those obtained experimentally. The model was extended by Broberg(1983) to include torsional and bending loads. Analytic models have the advantage of simplicity by identifying explicitly the major constituents of the disc (e.g., fiber, fluid). However, assumptions must be made to maintain simplicity, for example, interaction between fibres, or between the fibres and the ground substance cannot be easily accounted for.

The second general category of models are those which are based on numerical methods of mechanics. Analytic solutions to these complex models of the disc are generally not available. Thus a computational approach such as the finite element method has been used to obtain the solutions. Belytschko et al.(1974) constructed ~~an~~ axisymmetric model of the disc with adjacent truncated vertebral bodies, and studied its response under compression loads. The model included a linear fiber-reinforced composite description of the annulus. The model was extended to allow for nonlinear material response by Kulark et al.(1976). Lin et al.(1978) constructed a three-dimensional (3-D) model of the disc including a linear orthotropic description of the annulus (which was not related directly to fiber layer properties), and studied model response

under compression loading. Shirazi-Adl et al. (1984, 1985, 1986) also developed a 3-D model of the disc and adjacent truncated vertebral bodies, and studied response under compression, torsion and bending loads etc. In their model, fiber involvement in the annulus was included by superimposing a homogeneous isotropic material, representing the ground substance, and axial members, representing the fibres. They allowed for large (nonlinear) deformation and nonlinear material response. Ueno and Liu (1985) used a similar 3-D model with fibres modeled as cables (which cannot sustain compressive loads), and a commercial finite element program. They investigated model behaviour under different loads and the effects of variation in model material properties. However, a relatively coarse mesh was used because of the extensive representation of the substructures of the motion segment. Simmon et al. (1984) studied the transient response of a rhesus monkey motion segment by using a poroelastic representation and the corresponding finite element solution. Their approach recognizes the role of both solid and fluid components in the disc. Spilker et al. (1980, 1984, 1986) constructed a simple axisymmetric finite element model of a motion segment and carried out parametric studies of its response to axisymmetric compression. Modelling flexibility enabled extensive studies of the effects of disc geometry and tissue properties on behaviour. The model was later extended by Spilker et al. to allow nonaxisymmetric loading using a Fourier series representation which retained the computational advantages of a two-dimensional analysis. Spilker et al. further extended the model by incorporating an anisotropic description.

of the annular material, the annulus was considered to be a layered fiber-reinforced composite. The model was used to identify a set of layer material constants (linear) which could lead to model predictions in reasonable agreement with experimental measurements of gross segment motions under compression, torsion, shear, and bending loads.

2-2: TECHNICAL ASPECTS OF MODELING THE INTERVERTEBRAL DISC

Since the disc material exhibits both geometric and material nonlinearities, it is important that the analysis procedure is general in nature and capable of dealing with both types of nonlinearities simultaneously. The nucleus pulposus behaves as an incompressible inviscid fluid (Nachemson, 1960), so that the fluid-structure interaction has to be included in the analysis.

The problems of fluid-structure interaction can be categorized into different behaviour groups:

- (1) Interaction with large motion governed by fluid characteristics.
- (2) Interaction with relatively limited motion and short time duration, such as shock or impact.
- (3) Interaction with relatively limited motion and long time duration.

The present study considers the motion segment to experience static physiological motion and belongs to the third group mentioned above. Traditionally, these problems are solved in a two-step procedure (Sundqvist, 1983). First, the pressure predicted on a rigid model of the structure is solved using a finite-difference approach; then this pressure is applied to an elastic model of the structure in a finite-element model. This method has its drawbacks. For example, the pressure obtained is, in most cases, conservative and can lead to overestimation (Sundqvist, 1983). Recognizing the drawbacks, efforts have been directed to develop solution algorithms that directly solve the interactions between the fluid and the structure.

There are two methods of dealing with this. The Lagrangian displacement approach assumes three fundamental displacement unknowns at a node of a fluid element, while the pressure method assumes a scalar pressure unknown at a node of the fluid element. The pressure form has the disadvantage of resulting in a stiffness matrix without the symmetrical banding, but needs fewer degrees of freedom. The chief advantage of the displacement form is that interfaces to the structural elements are properly maintained because the procedure for formulation of the fluid element matrices is similar to that of the structural elements. However, a special constitutive law, which relates the stress and strain by the material matrix, must be defined for the fluid element. This study used the Lagrangian displacement formulation, since it is incorporated in the available finite element code, ADINA (Automatic Dynamic Incremental Nonlinear Analysis) at the University of Alberta.

2-3: A FLUID-STRUCTURE COMPATIBLE FORMULATION

In this analysis the motion of the body (both structural and fluid) in a fixed (stationary) Cartesian coordinate system is considered as displayed in Fig. 2.3-1. Bathe and Hahn (1979) developed a fluid-structure compatible formulation incorporated in the ADINA program. (All kinematic and static variables are measured in this coordinate system using tensor notation. Coordinates of a generic point, P, in the body at time 0 are ${}^0x_1, {}^0x_2, {}^0x_3$; at time t are ${}^tx_1, {}^tx_2, {}^tx_3$; and at time $t+\Delta t$ are ${}^{t+\Delta t}x_1, {}^{t+\Delta t}x_2, {}^{t+\Delta t}x_3$; where the left superscripts refer to the configuration of the body and the right subscripts to the coordinate axes. The notation for the displacement of the body is similar to the notation for the coordinates; namely, at time t the displacements are ${}^tu_i, i=1,2,3$ and at time $t+\Delta t$ the displacements are ${}^{t+\Delta t}u_i, i=1,2,3$. Therefore:

$${}^tx_i = {}^0x_i + {}^tu_i \quad [2.3-1]$$

$i=1,2,3$

$${}^{t+\Delta t}x_i = {}^0x_i + {}^{t+\Delta t}u_i \quad [2.3-2]$$

The increments in the displacements from time t to time $t+\Delta t$ are denoted as:

$$u_i = {}^{t+\Delta t}u_i - {}^tu_i \quad i=1,2,3 \quad [2.3-3]$$

During motion of the body, its volume, surface area, mass density, stresses, and strains are changing continuously. The specific mass, area, and volume of the body at time 0, t and $t+\Delta t$ are denoted as ${}^0\rho,$

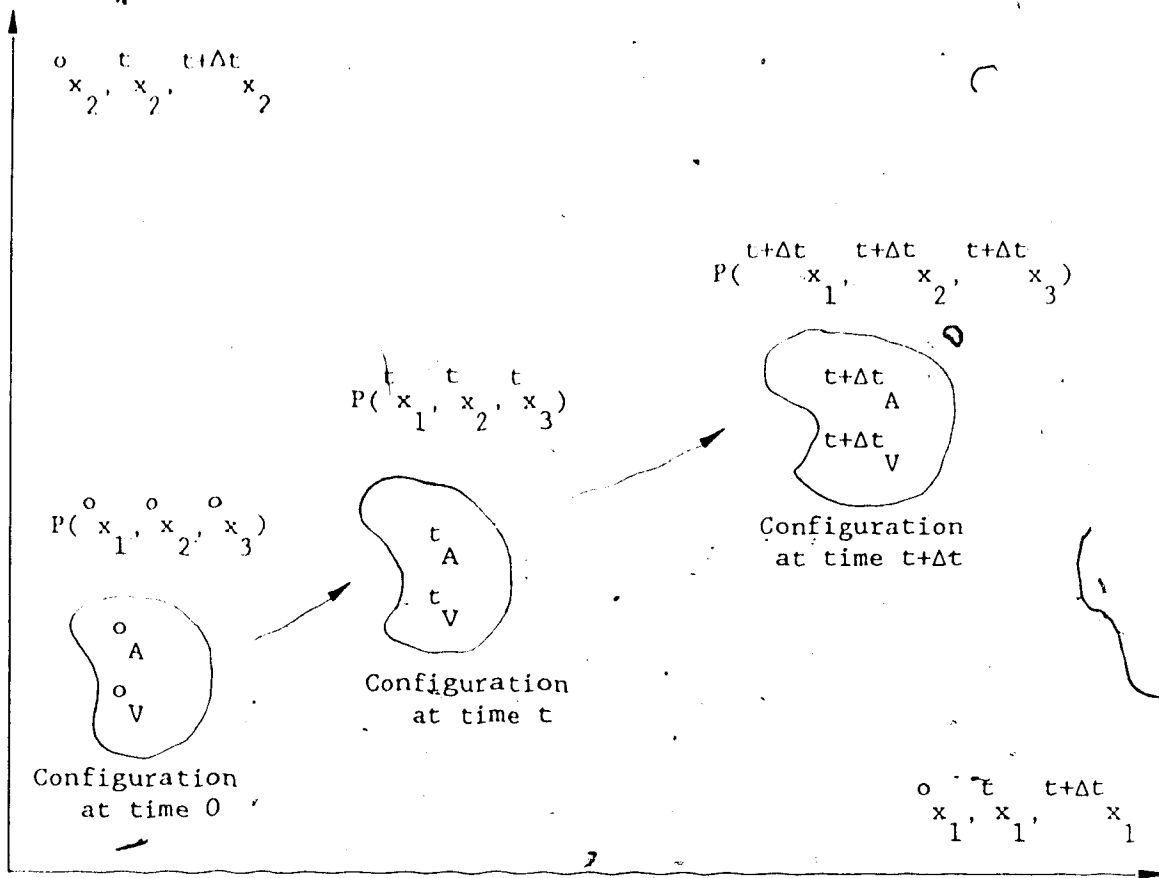


Figure 2.3-1: MOTION OF BODY IN STATIONARY CARTESIAN COORDINATE SYSTEM

t_ρ , $t+\Delta t_\rho$; o_A , t_A , $t+\Delta t_A$; and o_V , t_V , $t+\Delta t_V$; respectively. Analogous to the notation used for coordinates and displacements, a left superscript indicates the configuration in which the quantity (body force, surface traction, stress, etc.) being considered; in addition, a left subscript indicates the configuration with respect to which the quantity is measured. If the quantity under consideration occurs in the same configuration in which it is also measured, the left subscript may not be used; e.g., for the Cauchy stresses

$$\overset{t+\Delta t}{\sigma}_{ij} = \overset{t+\Delta t}{\sigma}_{ij}$$

In the formulation of the governing equilibrium equations derivatives of displacements and coordinates are required. In our notation a comma denotes differentiation with respect to the coordinate following, and the left subscript denoting time indicates the configuration in which this coordinate is measured for example,

$$\overset{t+\Delta t}{u}_{o\ i,j} = \frac{\overset{t+\Delta t}{u}_i}{\overset{o}{\partial x_j}}$$

and

$$\overset{o}{x}_{t+\Delta t\ m,n} = \frac{\overset{o}{\partial x_m}}{\overset{t+\Delta t}{\partial x_n}}$$

Using these conventions new symbols are defined when they are first encountered.

Using a Lagrangian formulation, in principle, a total or updated

formulation can be employed, but considering the numerical operations required for a fluid system, an updated Lagrangian (U.L.) formulation is more effective (Bath and Hahn, 1979). Consider a body of fluid or structure undergoing large deformations and assume that the solutions are known at all discrete times, namely $0, \Delta t, 2\Delta t, \dots, t$. The basic aim of the formulation is to establish an equation of virtual work from which the unknown static variables in the configuration at time $t+\Delta t$ can be solved. Since the displacement based finite element procedure is employed for numerical solution, the principle of virtual displacements is used to express the equilibrium of both structural and fluid bodies:

$$\int_{V_t} \delta \epsilon_{t,ij}^{t+\Delta t} S_{t,ij}^{t+\Delta t} dV = \delta E^{t+\Delta t} \quad [2.3-4]$$

in which $S_{t,ij}^{t+\Delta t}$ and $\epsilon_{t,ij}^{t+\Delta t}$ are the 2nd Piola-Kirchhoff stress tensor and Lagrangian-Green strain tensor respectively, which, at time $t+\Delta t$, are referred to the configuration time, t .

For a structural element:

$$S_{t,ij}^{t+\Delta t} = \frac{\rho}{t+\Delta t} \frac{\partial x_i}{\partial x_j} \sigma_{mn}^{t+\Delta t} \frac{\partial x_m}{\partial x_j} \quad [2.3-5]$$

and for a fluid element:

$$S_{t,ij}^{t+\Delta t} = \frac{\rho}{t+\Delta t} \frac{\partial x_i}{\partial x_j} (-p) \frac{\partial x_m}{\partial x_j} \quad [2.3-6]$$

For both structural and fluid elements:

$$\delta \epsilon_{ij}^{t+\Delta t} = \frac{1}{2} \delta (u_{i,j} + u_{j,i} + u_{k,i} u_{k,j}) \quad [2.3-7]$$

If incremental decomposition is introduced then the stress is given by:

$$\sigma_{ij}^{t+\Delta t} = \sigma_{ij}^t + S_{ij} \quad (\text{for structural element}) \quad [2.3-8]$$

$$\sigma_{ij}^{t+\Delta t} = -p \lambda_{ij} + S_{ij} \quad (\text{for fluid element}) \quad [2.3-9]$$

where λ_{ij} is the Kronecker delta; and the strain (for both structural and fluid elements), by:

$$\epsilon_{ij}^{t+\Delta t} = \epsilon_{ij}^t \quad [2.3-10]$$

$$\epsilon_{ij}^t = \epsilon_{ij}^e + \eta_{ij}^t \quad [2.3-11]$$

where

$$\epsilon_{ij}^e = \frac{1}{2} (u_{i,j} + u_{j,i}) \quad [2.3-12]$$

and

$$\eta_{ij}^t = \frac{1}{2} (u_{k,i} u_{k,j}) \quad [2.3-13]$$

Substituting equations [2.3-8] to [2.3-11] into the motion equation

[2.3-4] and using $\delta \epsilon_{ij}^t = \delta \epsilon_{ij}^e$ as well.

for a structural element:

$$\int_{t_V} \sigma_{ij}^t \delta \epsilon_{ij}^t dV + \int_{t_V} \sigma_{ij}^t \delta \eta_{ij}^t dV = \int_{t_V} \sigma_{ij}^t \delta \epsilon_{ij}^t dV$$

[2.3-14]

and for a fluid element:

$$\int_{t_V} S_{ij}^t \delta e_{t ij}^t dV - \int_{t_V} t_p^t \delta \eta_{t ii}^t dV = \int_{t_V} t_p^{t+\Delta t} \delta e_{t ii}^{t+\Delta t} dV \quad [2.3-15]$$

By using linear approximate equations;

for a structure element: $S_{ij}^t = C_{ijrs}^t e_{t rs}^t$; [2.3-16]

and for a fluid element : $S_{ij}^t = t_k^t e_{t mm}^t \lambda_{ij}$; [2.3-17]

The following approximate equations of motion are obtained;

for a structural element:

$$\int_{t_V} C_{ijrs}^t e_{t rs}^t \delta e_{t ij}^t dV + \int_{t_V} \sigma_{ij}^t \delta \eta_{t ij}^t dV = \int_{t_V} \sigma_{ij}^{t+\Delta t} \delta e_{t ij}^{t+\Delta t} dV \quad [2.3-18]$$

and for a fluid element:

$$\int_{t_V} t_k^t e_{t jj}^t \delta e_{t ii}^t dV - \int_{t_V} t_p^t \delta \eta_{t ii}^t dV = \int_{t_V} t_p^{t+\Delta t} \delta e_{t ii}^{t+\Delta t} dV \quad [2.3-19]$$

where t_{Cijrs} is the incremental material property tensor at time t referred to the configuration at time t . t_k is the fluid bulk modulus at time t referred to the configuration time t . $t_{\sigma ij}$ and t_p are the known Cauchy stress tensor and the pressure at time t . t_{eij} , $t_{\eta ij}$ are the

linear and nonlinear incremental parts of the Lagrangian-Green strain tensor referred to the configuration at time t .

The linearization procedure described above introduces errors in the solution, which may be large if the time step is relatively large. To reduce the solution errors and/or to avoid numerical instabilities, equilibrium iteration is used. The following equations are employed to solve for the incremental displacements;

for a structural element:

$$\int_{t_V} C_{ijrs}^t \Delta e_{rs}^{(k)} \delta e_{ij}^t dV + \int_{t_V} \sigma_{ij}^t \delta \Delta \eta_{ij}^{(k)} dV$$

$$= \frac{t+\Delta t}{t} E - \int_{t+\Delta t_V} \sigma_{ij}^{(k-1)} \delta e_{ij}^{(k-1)} dV$$

[2.3-20]

for a fluid element:

$$\int_{t_V} t_k \Delta e_{jj}^{(k)} \delta e_{ii}^t dV - \int_{t_V} t_p \delta \Delta \eta_{ii}^{(k)} dV$$

$$= \frac{t+\Delta t}{t} E + \int_{t+\Delta t_V} p^{(k-1)} \delta e_{ii}^{(k-1)} dV$$

[2.3-21]

where

$$u_j^{t+\Delta t (k)} = u_j^{t+\Delta t (k-1)} + \Delta u_j^{(k)}$$

[2.3-22]

(note: equations [2.3-21], [2.3-22] reduce to [2.3-19], [2.3-20] when

$k=1$)

Using finite element discretization, the basic assumptions for an element are:

$$x_i^t = \sum_{k=1}^n h_k^t x_i^k \quad [2.3-23]$$

$$u_i^t = \sum_{k=1}^n h_k^t u_i^k \quad i=1,2,3 \quad [2.3-24]$$

$$\Delta u_i^t = \sum_{k=1}^n h_k^t \Delta u_i^k \quad [2.3-25]$$

where n is the number of nodes of the element being considered, h_k^t are the element interpolation functions, and the x_i^t , u_i^t and Δu_i^t are the coordinates, displacements and incremental displacements of the nodal point k at time t . Substituting the relations in equations from [2.3-23] to [2.3-25] into equations [2.3-20], [2.3-21] and adding them together, the governing finite element equations are obtained:

$$\left[\begin{matrix} K_L \\ K_{NL} \end{matrix} \right]^t \Delta U^{(i)} = \begin{matrix} t+\Delta t \\ t+\Delta t \end{matrix} R - \begin{matrix} t+\Delta t \\ t+\Delta t \end{matrix} F^{(i-1)} \quad [2.3-26]$$

The terms on equation [2.3-26] are:

$\begin{matrix} K_L \\ K_{NL} \end{matrix}^t$: linear, nonlinear stiffness matrix in the configuration at time t .

ΔU : vector of incremental nodal point displacements.

$\begin{matrix} t+\Delta t \\ R \end{matrix}$: vector of external loads at time $t+\Delta t$.

$\begin{matrix} t+\Delta t \\ F \end{matrix}$: vector of nodal point forces at time $t+\Delta t$.

and the superscript (i) indicates "i"th iteration.

TABLE 2.3-1: FINITE ELEMENT MATRICES FOR UPDATED LAGRANGIAN FORMULATION.

Integral	Matrix Evaluation
${}^{t+\Delta t}R = \int_{o_A} {}^{t+\Delta t} \begin{matrix} s & s & o \\ f & \delta u & \\ 0 & i & i \end{matrix} dA$ $+ \int_{o_V} {}^{t+\Delta t} \begin{matrix} b & \\ f & \delta u & o \\ 0 & i & i \end{matrix} dV$	${}^{t+\Delta t}R = \int_{o_A} {}^{t+\Delta t} \begin{matrix} s^T & t+\Delta t & s & o \\ H & f & \\ 0 & & \end{matrix} dA$ $+ \int_{o_V} {}^{t+\Delta t} \begin{matrix} T & t+\Delta t & b & o \\ H & f & \\ 0 & & \end{matrix} dV$
$\sum_{m=1}^p \int_{t_V} {}^t C_{ijrs} {}^t e_{rs} \delta {}^t e_{ij} dV$ $+ \sum_{h=1}^q \int_{t_V} {}^t k_{ijrs} \lambda_{ijrs} {}^t e_{rs} \delta {}^t e_{ij} dV$	${}^t K_L = \sum_{m=1}^p \int_{t_V} {}^t \begin{matrix} T & t & t \\ B & C & B \\ t & L & t \end{matrix} dV$ $+ \sum_{h=1}^q \int_{t_V} {}^t \begin{matrix} T & t & t \\ B & k & B \\ t & L & t \end{matrix} dV$
$\sum_{m=1}^p \int_{t_V} {}^t \sigma_{ij} \delta {}^t \eta_{ij} dV$ $+ \sum_{h=1}^q \int_{t_V} {}^t p_{ij} \lambda_{ij} \delta {}^t \eta_{ij} dV$	${}^t K_{NL} = \sum_{m=1}^p \int_{t_V} {}^t \begin{matrix} T & t & t \\ B & \Gamma & B \\ t & NL & t \end{matrix} dV$ $+ \sum_{h=1}^q \int_{t_V} {}^t \begin{matrix} T & t & t \\ B & -p & B \\ t & NL & t \end{matrix} dV$
$\sum_{m=1}^p \int_{t+\Delta t_V} {}^{t+\Delta t} \sigma_{ij} \delta {}^{t+\Delta t} e_{ij} dV$ $+ \sum_{h=1}^q \int_{t+\Delta t_V} {}^{t+\Delta t} p_{ij} \lambda_{ij} \delta {}^{t+\Delta t} e_{ij} dV$	${}^{t+\Delta t} F = \sum_{m=1}^p \int_{t+\Delta t_V} {}^{t+\Delta t} \begin{matrix} T & t+\Delta t & t+\Delta t \\ B & \Gamma & B \\ t+\Delta t & L & t+\Delta t \end{matrix} dV$ $+ \sum_{h=1}^q \int_{t+\Delta t_V} {}^{t+\Delta t} \begin{matrix} T & t+\Delta t & t+\Delta t \\ B & -p & B \\ t+\Delta t & L & t+\Delta t \end{matrix} dV$

The following notation is used for calculation of the element matrices:

$^s H, ^v H$: Surface and volume displacement interpolation matrices.
 $^{t+\Delta t}_0 f^s, ^{t+\Delta t}_0 f^v$: Vector of surface and body forces defined per unit area and per unit volume of the element at time 0.

$^t_{tL} B, ^t_{tNL} B$: Linear and nonlinear strain-displacement transformation matrices.

$^t C$: Stress-strain material property matrix.

$^t \Gamma$: Matrix of Cauchy stresses.

p : Number of structural elements.

q : Number of fluid elements.

Using the above formulation, 8 nodal 3-D elastic and fluid elements, 2 nodal cable elements are used by ADINA in three dimensional analysis of vertebral motion segment.

2-4: SOME ASPECTS CONCERNING MATERIAL AND GEOMETRIC PROPERTIES

The finite element grid used in this study corresponds to the general geometry of a lumbar body-disc-body assuming symmetry across the sagittal plane. Table 2.4-1 lists the overall dimensions of the grid (Shirazi-Adl. et al, 1984). The posterior elements, ligaments and muscles are not included in the present model. Thirty two 8-node, 3-D inviscid, incompressible elements were used for the nucleus pulposus; eighty 8-node, 3-D elastic elements for the cortical bone; 144 8-node 3-D elastic elements for the cancellous bone; and 112 8-node 3-D elastic elements for the bony end-plate. The annulus fibrosus is represented by 144 2-node nonlinear elastic cable elements (collagenous fibres) embedded in 80 8-node 3-D elastic element (ground substances).

TABLE 2.4-1: OVERALL DIMENSIONS OF THE LUMBAR VERTEBRAL MODEL

Diameters (mm)		Disc thickness (mm)	Cross-sectional area (mm ²)	
Lateral	Sagittal		Disc	Nucleus
48.0	34.0	10.0	1369.250	710.462

The incompressibility of the nucleus pulposus is accomplished by imposing a large bulk modulus t_α in a linear relation between pressure and volumetric strain.

$$t_p = -t_\alpha \frac{\Delta V}{V_0}$$

[2.4-1]

in which α is four orders of magnitude larger than the other stiffness terms. The annulus is modelled as a composite material of collagenous fibres embedded in a matrix of ground substance. A collagenous fiber content of 16% of annulus volume was assumed (Galante, 1967). The collagenous fibres are distributed through six layers. The ratio of the cross-sectional area is listed in Table 2.4-2 (Brickley-Parsons and Glimcher, 1984).

TABLE 2.4-2: DISTRIBUTIONS OF THE COLLAGENOUS FIBRES AMONG LAYERS

	Layer 1 and 2	Layer 3 and 4	Layer 5 and 6
Ratio of cross-sectional area:	1.0	0.7	0.42

Fig 2.4-1 shows the stress-strain curve for the collagenous fibres in the disc. This curve is based on the results reported by a number of investigators (Abrahams, 1967, Sanjeevi et al., 1982, Haut et al., 1972). The material properties used for the bony parts and the annulus ground substance are listed in Table 2.4-3. The bony parts are modeled by homogeneous, elastic elements with different material properties for cortical bone, cancellous bone and end-plate. In view of the small strains experienced by the bony elements, it is assumed that they obey a relation that does not depend on the state of strain. The generalized Hooke's law is employed:

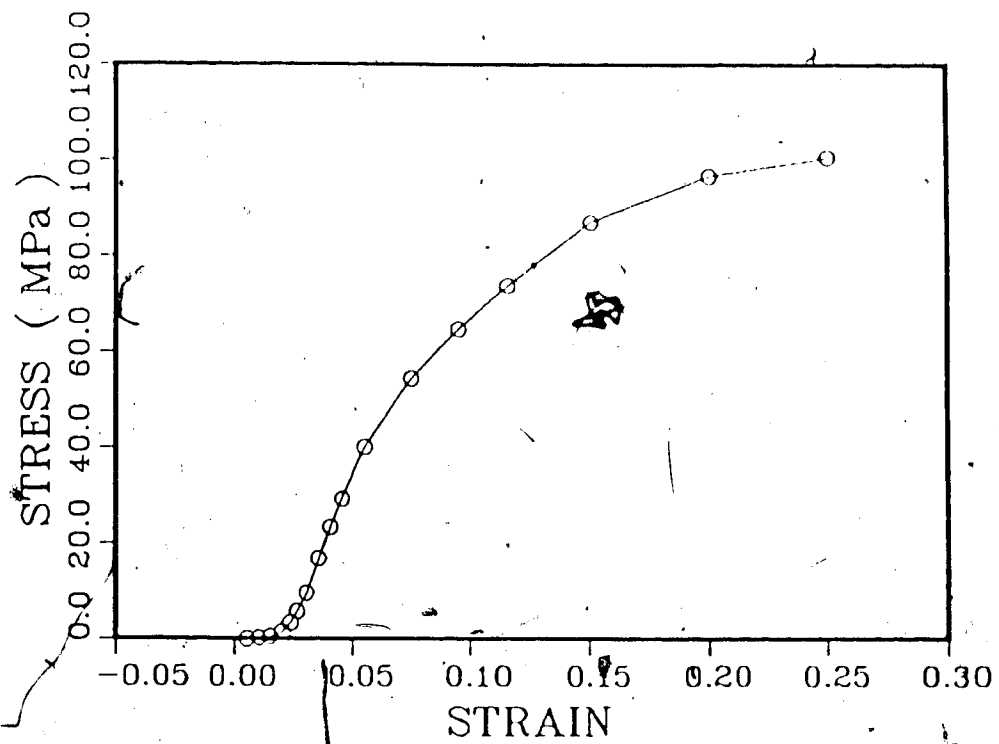


Figure 2.4-1: CONSTITUTIVE CURVE FOR THE COLLAGENOUS FIBER

$$t_{Cijrs} = \phi \lambda_{ij} \lambda_{rs} + \mu (\lambda_{ir} \lambda_{js} + \lambda_{is} \lambda_{jr}) \quad [2.4-2]$$

where ϕ and ν are the Lamé constants and λ_{ij} is the Kronecker delta, and

$$\phi = \frac{E \nu}{(1 + \nu)(1 - 2\nu)} \quad [2.4-3]$$

$$\mu = \frac{E}{2(1 + \nu)} \quad [2.4-4]$$

The material properties of the annulus ground substance were extracted from the initial portion of the stress-strain curve on the basis that initially the ground substance is the main carrying component of the annulus fibrosus (Wu and Yao, 1976).

TABLE 2.4-3: MATERIAL PROPERTIES OF THE BONY PARTS AND THE ANNULUS

	Modulus of elasticity (MPa)	Modulus of rigidity (MPa)	Poisson's ratio	
Cortical bone	12000.0	4615.0	0.3	Brown et al.(1981) Burstein et al.(1976) Evans (1973) Shirazi-Adl et al. (1984)
Cancellous bone	100.0	41.7	0.2	Lindahl (1975) Yamada (1970) Shirazi-Adl et al. (1984)
Ground Substance (Annulus)	4.2	1.6	0.45	Yamada (1970) Wu and Yao (1976) Shirazi-Adl et al. (1984)

2-5: LOADING AND BOUNDARY CONDITIONS

Compression, axial torsion, flexion, extension and lateral bending loads were separately applied to the body-disc-body model. As the posterior parts, the ligaments, and the muscles are not included in the present model, the numerical results obtained simulates the behaviour of the body-disc-body unit only.

The finite element mesh includes a disc and two adjacent vertebrae (Fig.2.5-1). The inferior vertebra is truncated. Since under axial torsion, flexion, extension and lateral bending, the rotation centre and the distribution of the stresses in the vertebra is unknown. It is important, because of Saint-Venant's principle, to include a sufficient length of vertebra to allow the transmission of the stresses through the endplate. Consequently, a total vertebra is built on the top of the disc. The fixed boundary condition is applied at the bottom of the underlying truncated vertebra.

The axial torque, flexion, extension and lateral bending moment are represented by distributed load on the cortical bone at the top of the upper vertebra. This is based on the knowledge that the cortical bone is the major bony part to withstand loading. The elastic modulus of the cortical bone is comparatively larger than that of the cancellous bone (Yamada, 1970).

An axial torque of 10 N·m is represented by a linearly varying distribution of horizontal loads (in both X and Y directions) acting on the top of the upper vertebra and causing zero net shear forces (Fig. 2.5-2).

Flexion, extension and the lateral bending moments of magnitude 10 N·m are represented by similar loads in the X and Y direction respectively (Fig. 2.5-3, 2.5-4, 2.5-5).

This torque (10 N·m) is greater than a normal value physiologically applied torque on the motion segment (White and Panjabi, 1978).

In compression, since the vertebral body is stiff compared to the disc, the vertebral rigidity is modeled as a boundary condition in which the surface of the vertebra is applied as a uniform displacement load, corresponding to a compressive load of 1600 N.

Loads are increased incrementally from zero to their maximum values.

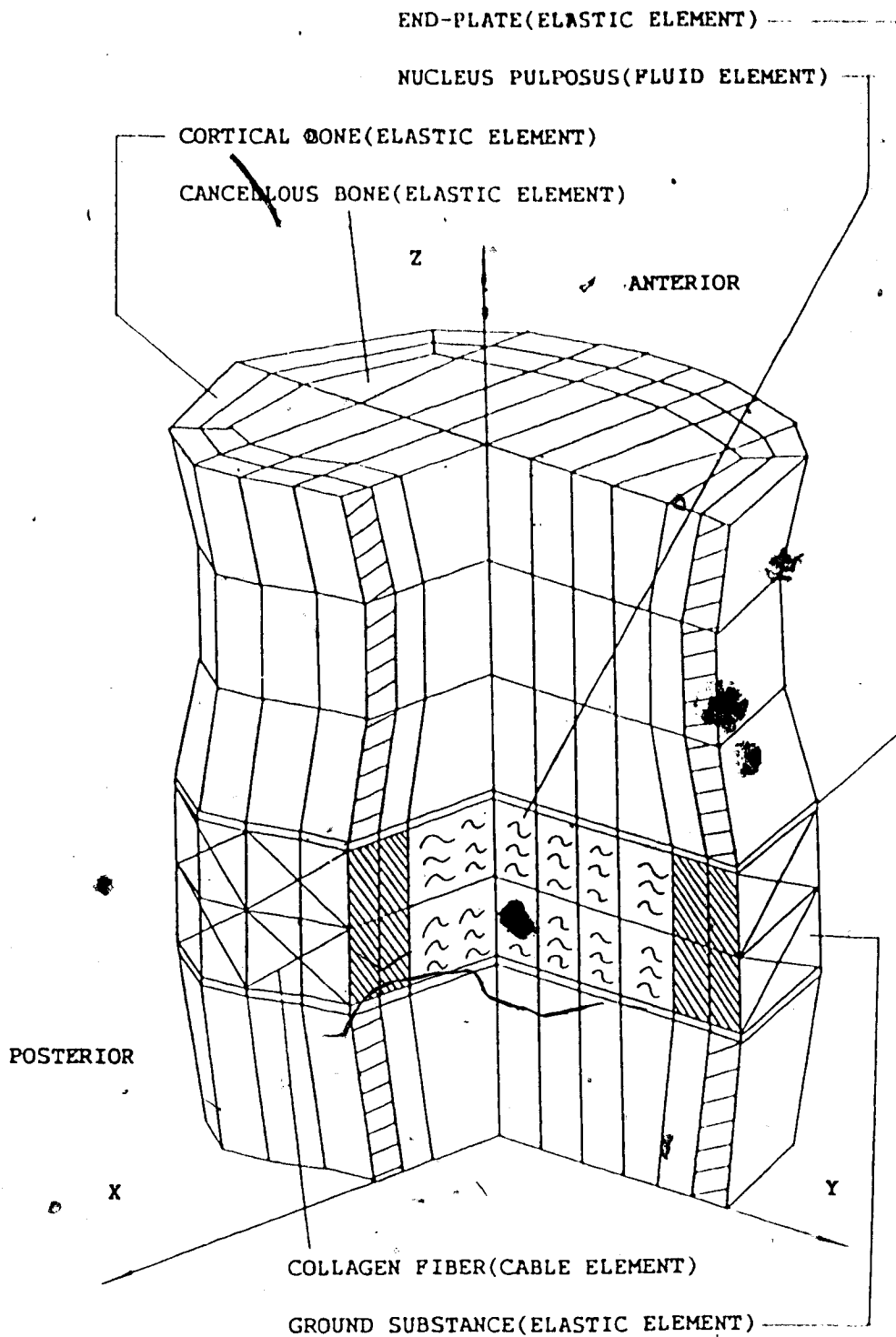


Figure 2.5-1: OUTLINE OF THE PRESENT FINITE ELEMENT MODEL.

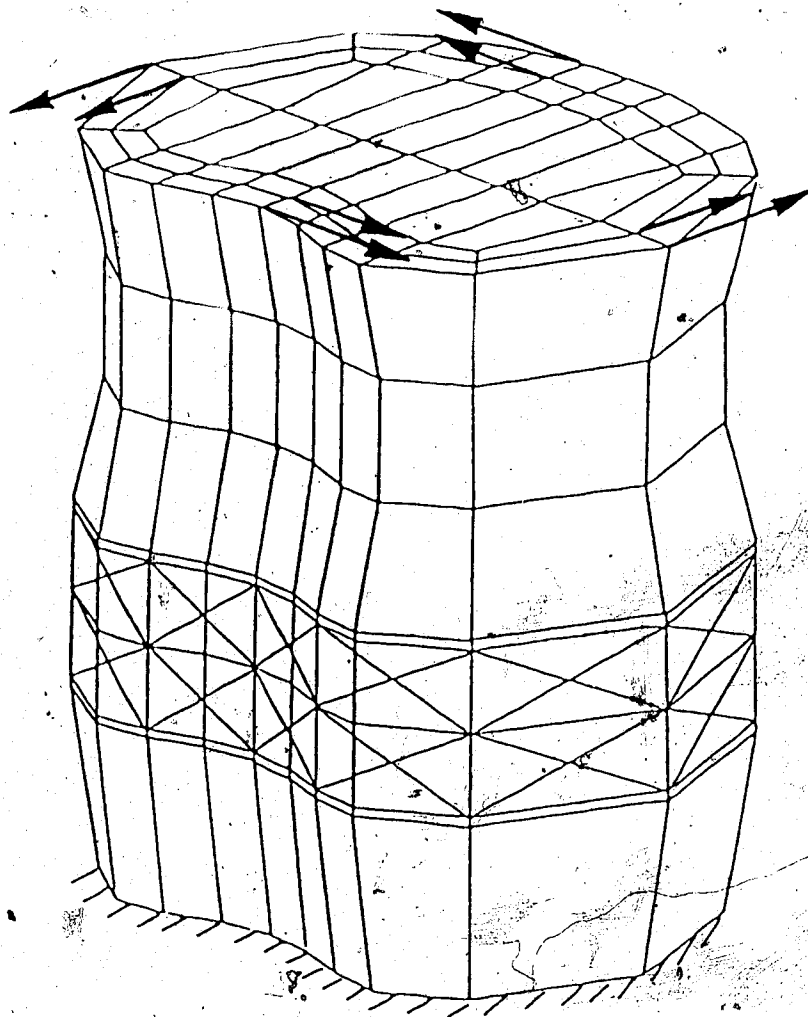


Figure 2.5-2: POSTEROLATERAL VIEW OF THE PRESENT MODEL
(Under axial torsion)

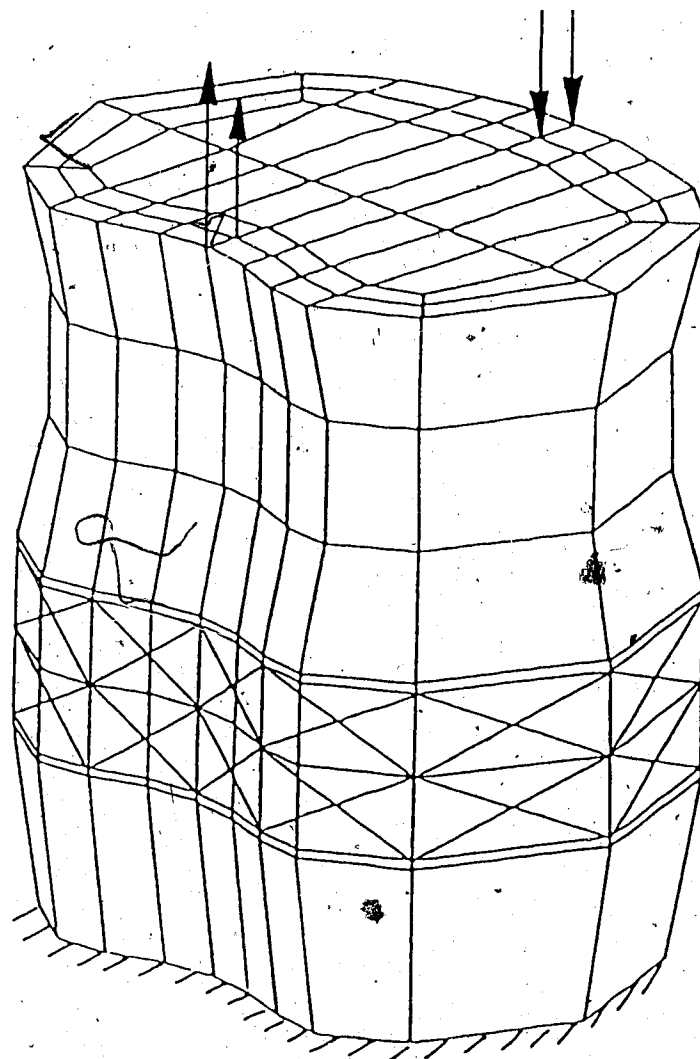


Figure 2.5-3: POSTEROLATERAL VIEW OF THE PRESENT MODEL
(Under flexion)

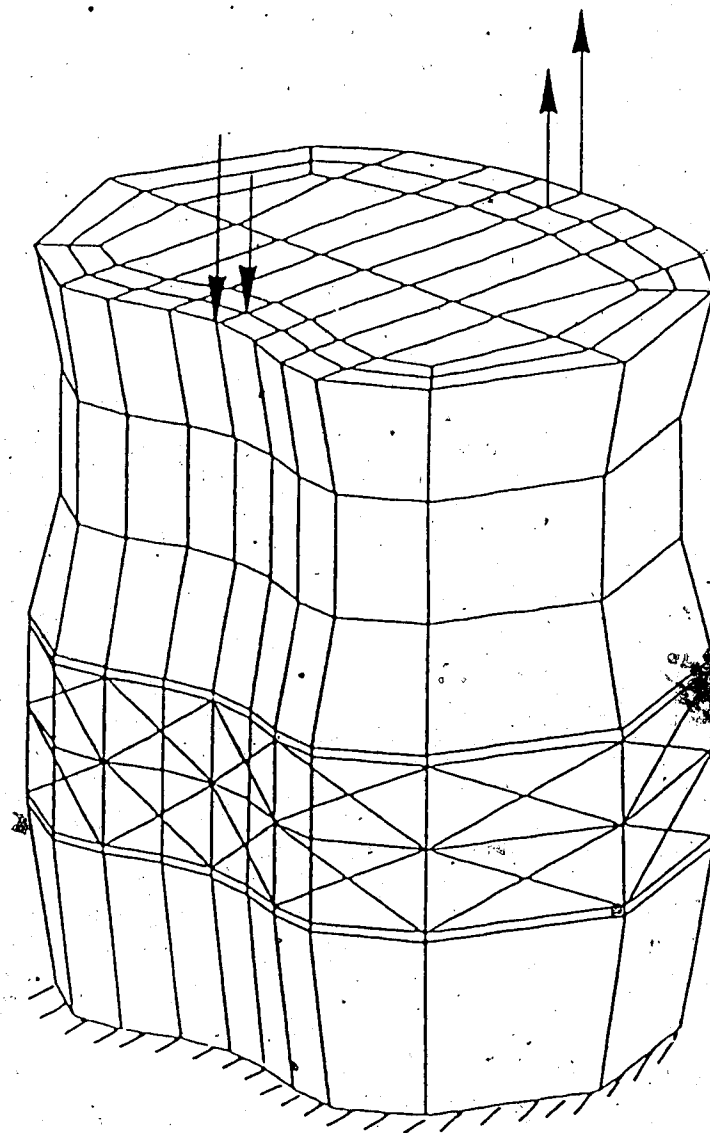


Figure 2.5-4: POSTEROLATERAL VIEW OF THE PRESENT MODEL
(Under extension)

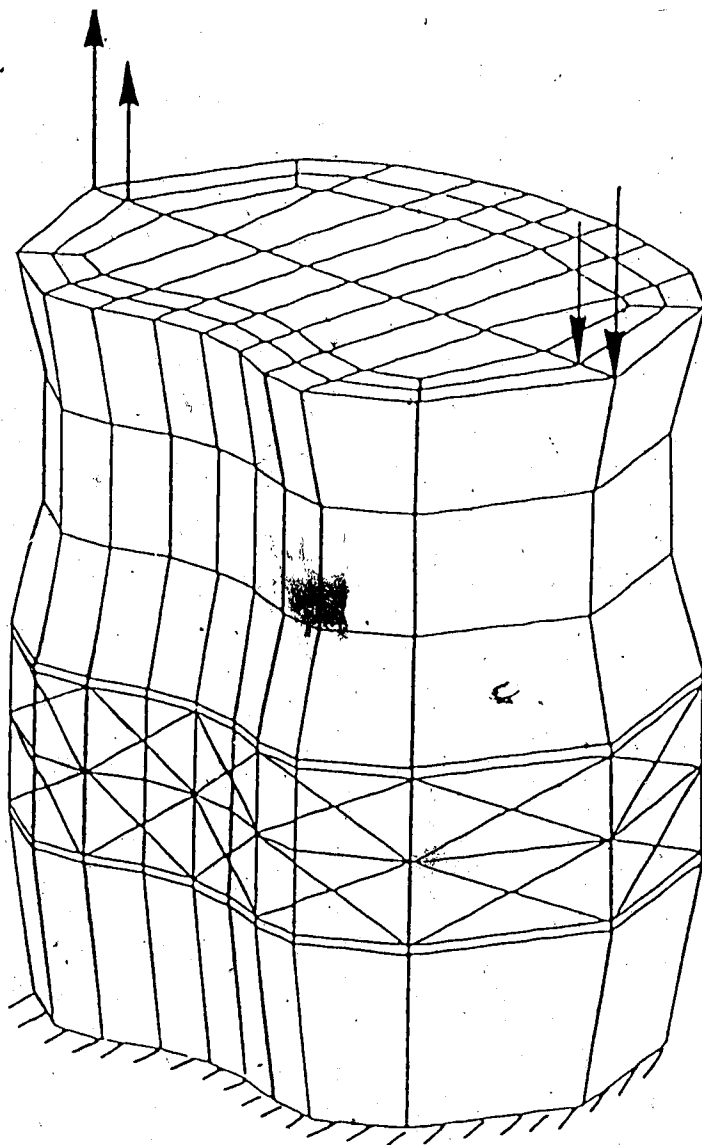


Figure 2.5-5: POSTEROLATERAL VIEW OF THE PRESENT MODEL
(Under right lateral bending)

CHAPTER 3: NUMERICAL RESULTS

3-1: VALIDATION OF THE FINITE ELEMENT MODEL

Since analytical solutions for motion segment response are not available, the best way to verify the model is to compare present predictions with those obtained from experimental work. The most complete data in the published literature describes disc-body (truncated) unit response under compressive load and are presented in terms of gross displacement behaviour (Virgin, 1951; Markolf, 1972; Markolf and Morris, 1974), or intradiscal pressure (Rolander, 1966; Ranu et al, 1979).

In comparing present predictions with experimental results, the emphasis has been placed on results obtained from lumbar intervertebral motion segments tested without posterior elements. It needs to be stressed that published results exhibit considerable scatter. Tencer and Ahmed (1981) noted that such discrepancies are not only due to unavoidable biologic variation among specimens, but also to differences in the experimental techniques and methods employed by different investigators. However, the experimental work agrees qualitatively.

Fig. 3.1-1 shows the predicted vertical displacement of the disc under compression. The stiffening effect of increasing load on the disc is evident; due primarily, to the collagenous fibers of the annulus.

These fibers are subjected to tensile strain as a result of transverse bulging of the disc and present stiff constitutive behaviour in tension (Abrahams, 1967). This effect resists further horizontal deformation and hence additional vertical displacement of the disc. Moreover, the increase in the cross-sectional area of the whole disc, the decrease in the slope (with respect to the horizontal plane) of the annulus fibers, and an increase in the generated nucleus pressure, all contribute to the stiffening behaviour of the disc with compressive load. It can be seen that the present model provides results similar to those from "in vitro" measurements.

Variation of intradiscal pressure with compressive load from the collected results of "in vitro" measurements are compared in Fig. 3.1-2. Although gross displacement behaviour of the disc tends to be nonlinear, intradiscal pressure increases in a nearly linear manner with increasing compressive load. This implies that substitution can be made by a distributed pressure applied on the walls of the annulus and the bony end-plate, the nucleus is not analyzed. The pressure can be represented as a linear function of the increasing compressive load.

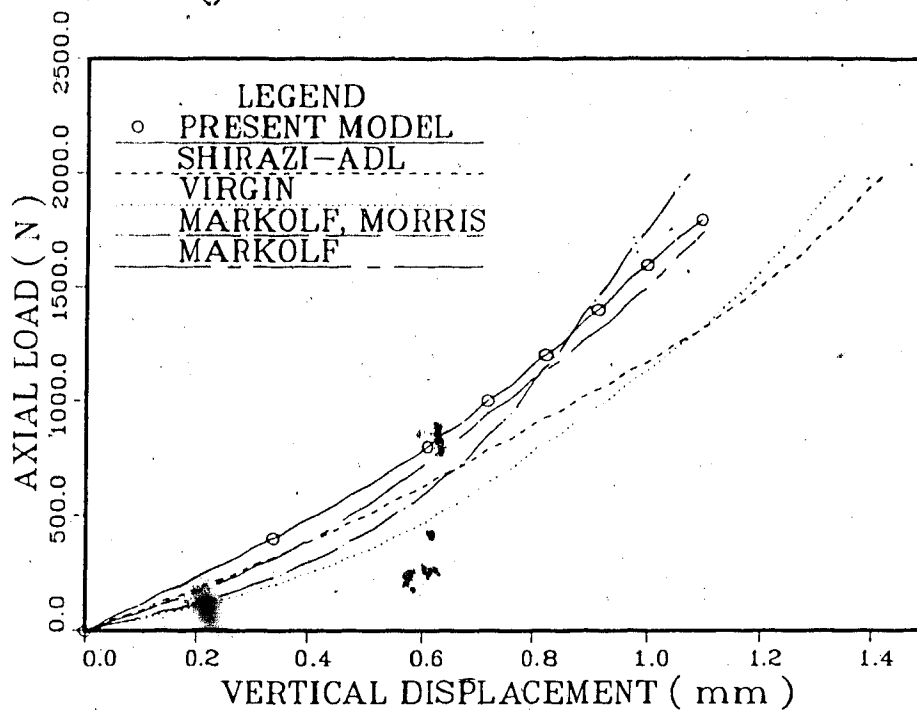


Figure 3.1-1: DISC BEHAVIOUR UNDER COMPRESSION

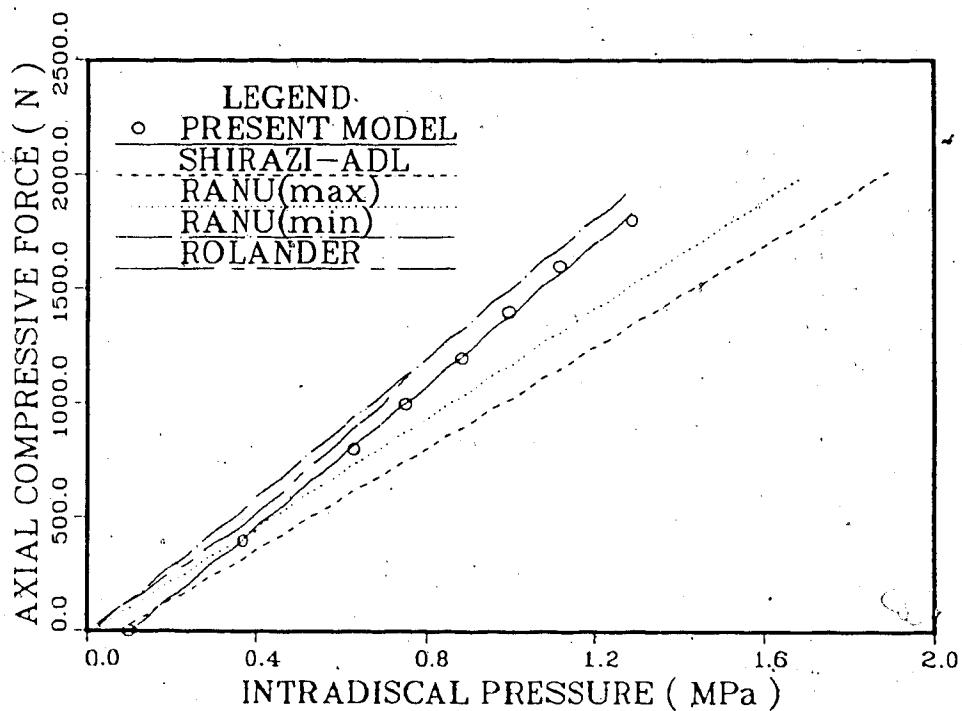


Figure 3.1-2: INTRADISCAL PRESSURE UNDER COMPRESSION

3-2: STRESS DISTRIBUTION ON THE END-PLATE

As mentioned in §1-8, one challenge of modeling spine fixation systems deals with a correct specification of the intradiscal boundary conditions. Since the end-plate, anatomically, is the interaction region between the disc and the vertebra, predictions of the stress distribution on an internal end-plate and the end-plate deformation from a multiple body model may subsequently be used for intradiscal boundary conditions. The loading style on future spine fixation systems can be defined in this way.

Nondimensional X coordinates are defined for convenience of comparing the stresses σ_{ij} , because sagittal diameters change across the intervertebral body. Distance from the origin to the periphery is 1 and each element length is 0.333. In this nondimensional coordinates system, -1.0 to -0.667 and 0.667 to 1 refer to the cortical region; -0.667 to 0.667 refer to the cancellous bone; -1.0 to -0.333 and 0.333 to 1.0 refer to the annulus; and -0.333 to 0.333 refers to the nucleus region (Fig. 3.2-1).

Fig. 3.2-1 shows the normal stress σ_{zz} transmission through the intervertebral body along the X axis. The stress was defined at the Gauss integration output points in the vertebral elements. It can be seen that σ_{zz} is uniformly distributed on the end-plate adjacent to the nucleus. This uniformity agrees with the assumption that the nucleus is incompressible. On the outer boundary of the end-plate, adjacent to the posterior and anterior regions, σ_{zz} is greater than those on the central region of the end-plate. This change starts in the interaction

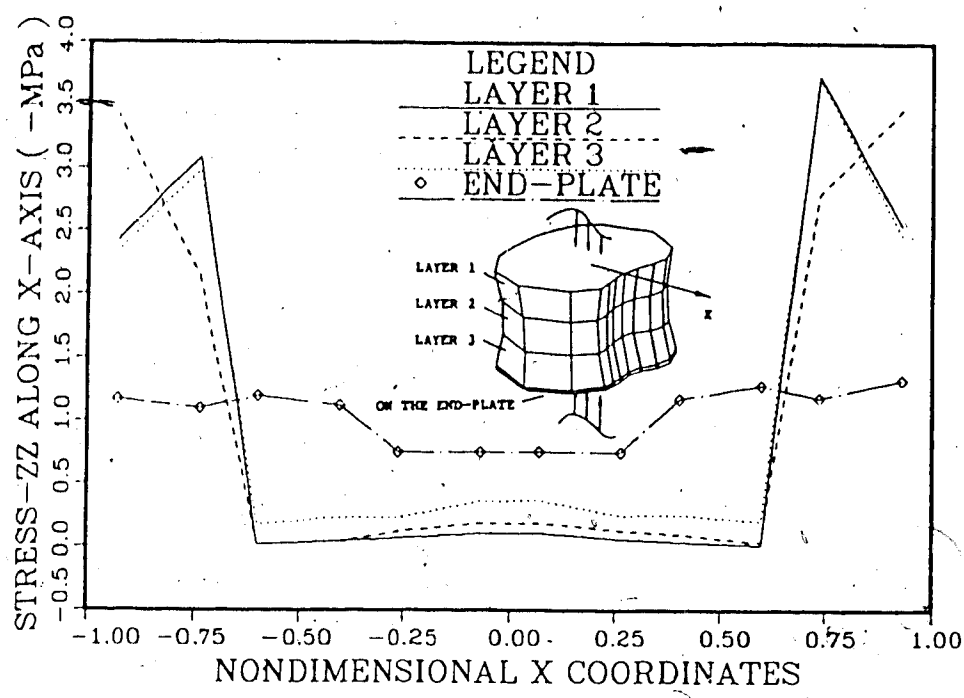
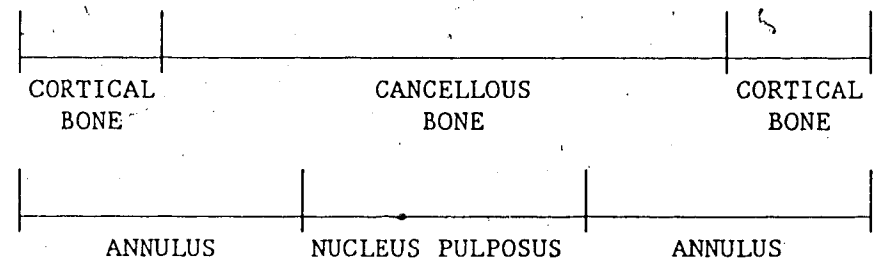


Figure 3.2-1: NORMAL STRESS σ_{zz} TRANSMISSION THROUGH THE VERTEBRAL BODY
(Under compression)



region between the nucleus and the annulus (nondimensional X coordinates equal to -0.333 or 0.333). This distribution results from the fact that the elastic modulus of the cortical bone is comparatively larger than that of the cancellous bone. The stiffer the component is, the larger proportion of load it will carry.

Fig. 3.2-2 shows the shear stress σ_{zx} distribution along the X axis. It is apparent that the shear stress is zero on the central end-plate region, adjacent to the nucleus pulposus. This is not surprising since the nucleus pulposus was assumed to be an inviscid fluid. This plot reflects the restriction of the vertebra on the horizontal bulging of the intervertebral disc. This restriction exists primarily around the perimeter of the end-plate. Due to the geometry of the intervertebral disc, the shear stress σ_{zx} is greater at the posterior part (with positive X coordinates) than at anterior part (with negative X coordinates). This implies that more restriction occurs at the posterior part preventing the disc from horizontally bulging.

Fig. 3.2-3 to Fig. 3.2-5 show the normal stress σ_{zz} transmission through the vertebra under flexion, extension, and right lateral bending. Fig. 3.2-6 indicates the shear stress σ_{zy} transmission under axial rotation. It can be seen that through the vertebral body, both the normal stress σ_{zz} and shear stress σ_{zy} distribute gradually from noncontinuous curve (layer 1 or 2) to continuous one (on the end-plate). This means that vertebral body height is sufficiently great to allow the uniform distribution of stresses through the layers.

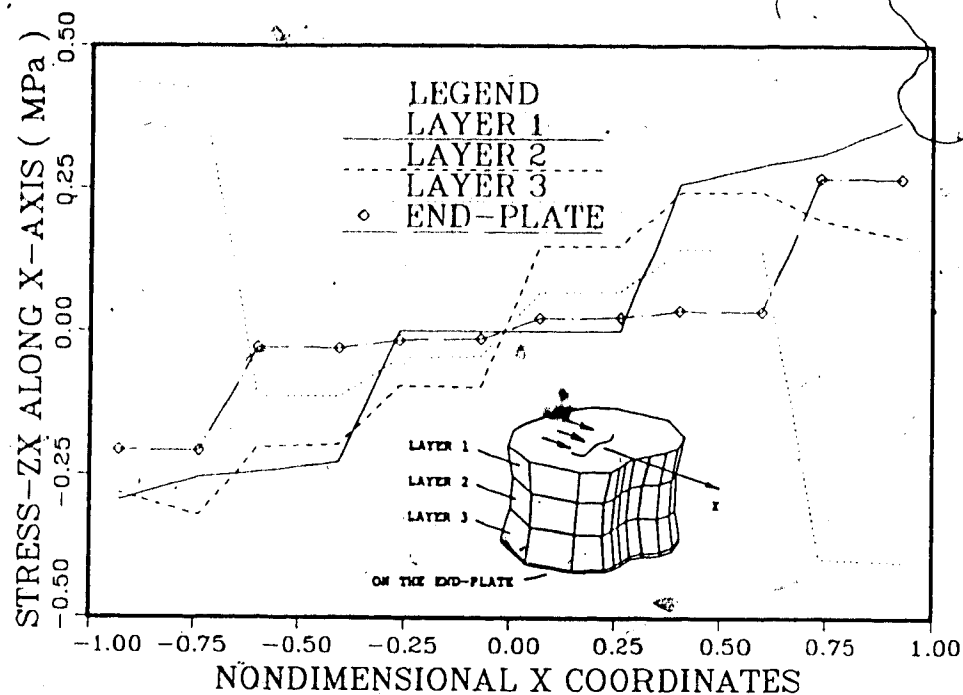


Figure 3.2-2: SHEAR STRESS σ_{zx} TRANSMISSION THROUGH THE VERTEBRAL BODY
(Under compression)

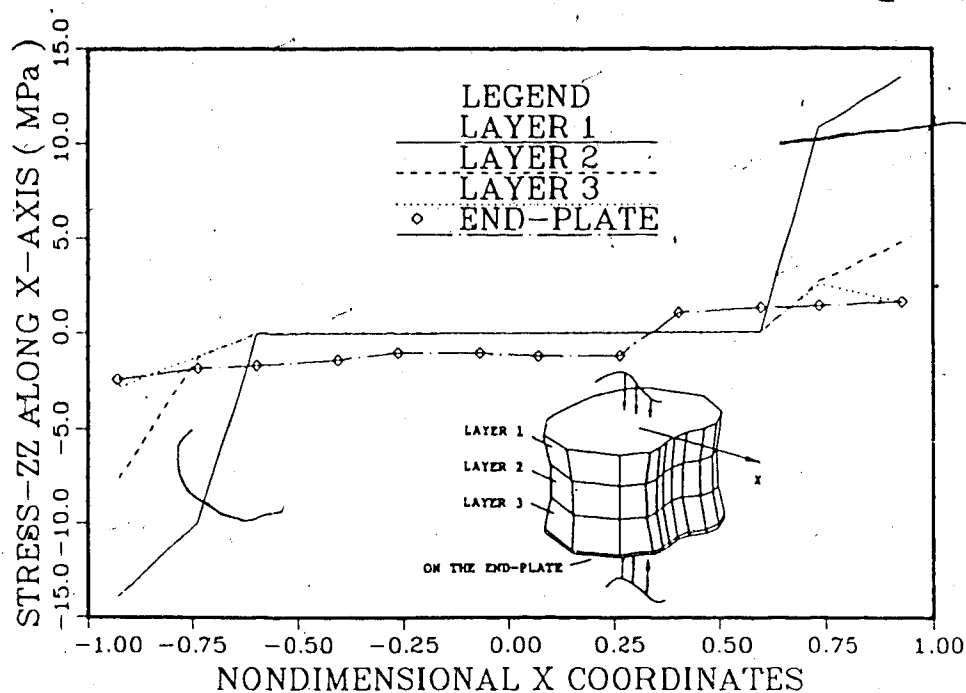


Figure 3.2-3: NORMAL STRESS σ_{zz} TRANSMISSION THROUGH THE VERTEBRAL BODY
(Under flexion)

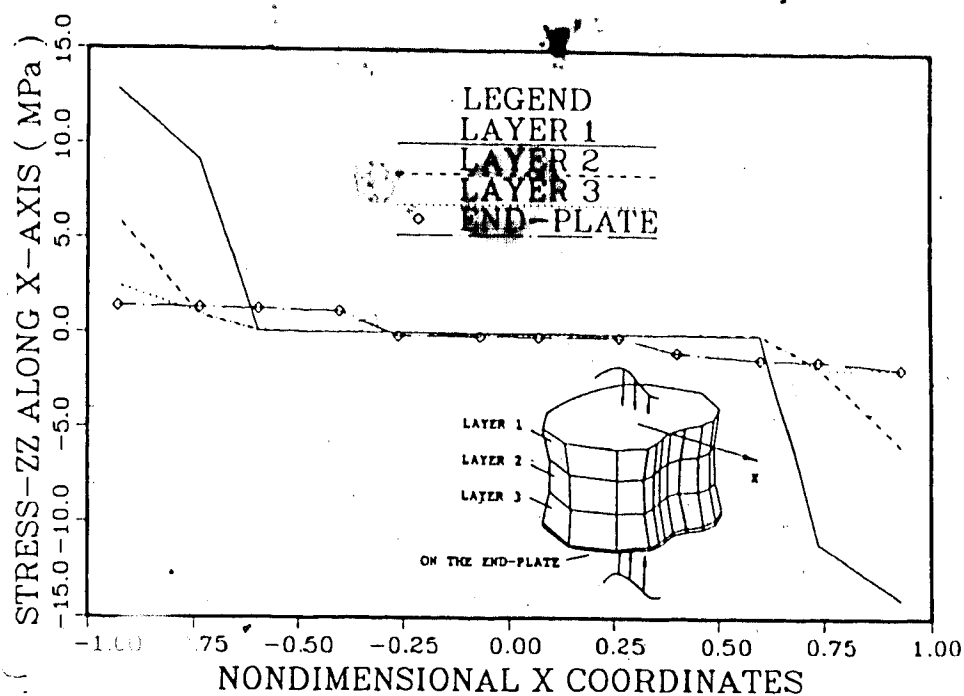


Figure 3.2-4: NORMAL STRESS σ_{zz} TRANSMISSION THROUGH THE VERTEBRAL BODY
(Under extension)

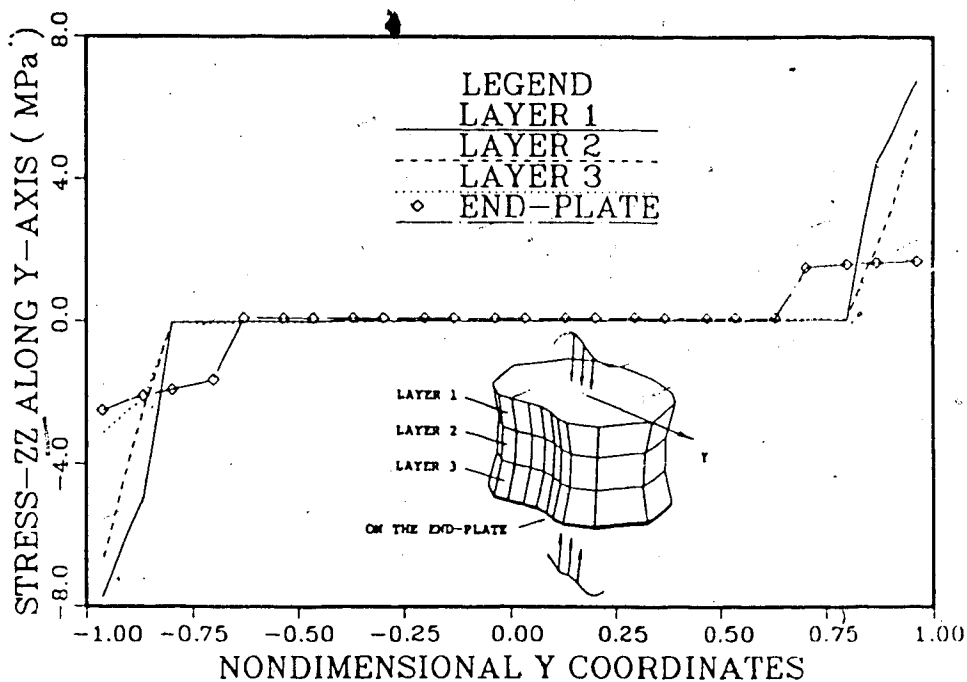


Figure 3.2-5: NORMAL STRESS σ_{zz} TRANSMISSION THROUGH THE VERTEBRAL BODY
(Under right lateral bending)

Fig. 3.2-3 to Fig. 3.2-6 indicate the general phenomenon of either normal stress σ_{zz} (compression, flexion, extension and lateral bending) or shear stress σ_{zy} (axial torsion) distribution: the stresses distribute uniformly in the central end-plate region; Starting from the interface of the nucleus and the annulus, the stresses increase and nearly uniform through the outer border. The periphery end-plate region, adjacent to the annulus pulposus, bears a larger amount of load than the central end-plate region.

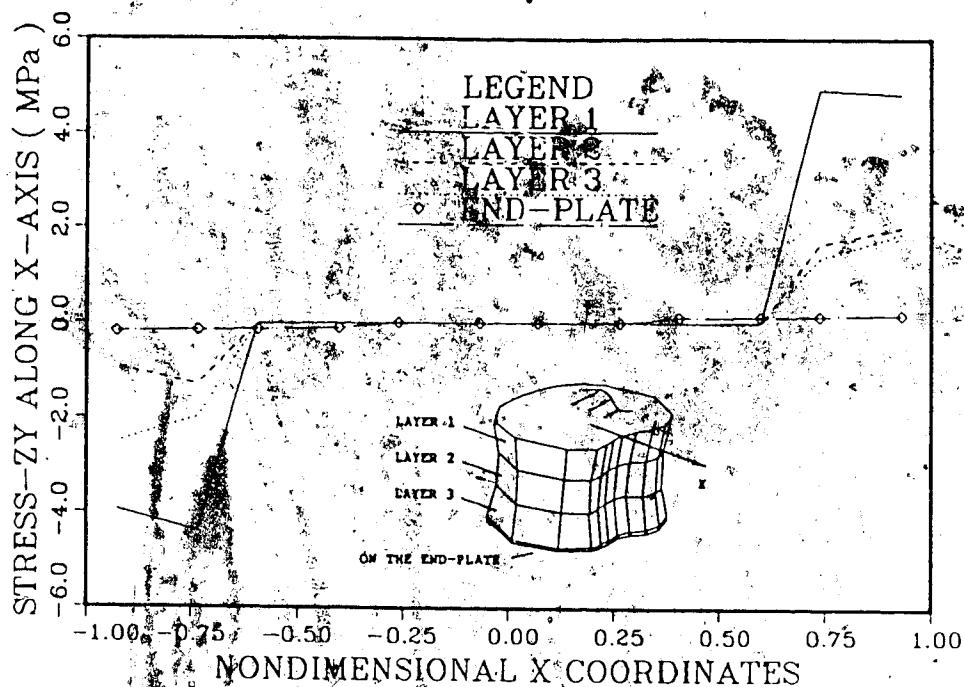


Figure 3.2-6: SHEAR STRESS σ_{zy} TRANSMISSION THROUGH THE VERTEBRAL BODY
(Under axial torsion)

3-3: END-PLATE DEFORMATION


Fig. 3.3-1 shows the end-plate upward bulging under compression. A nondimensional bulging parameter B/D was defined as the ratio of maximum end-plate bulge to disc height decrease. In Fig. 3.3-2, B/D is nearly linear versus the increasing compressive load. End-plate bulging phenomenon was also experimentally measured by Rolander and Blair (1975), Reuber et al (1980). The nondimensional parameter B/D can be used for specifying the displacement boundary conditions for spine fixation systems. When the load is small, the contributions of the vertebrae on the top and bottom of our spine fixation systems can be represented by a rigid body. However, with the compressive load increases, a convex shape for the end-plate  be specified.

Fig. 3.3-3 shows the sagittal end-plate deflection under compression, extension and flexion. The bony end-plate deflected as a rigid body for a compression load of 1000 N. Results were also obtained when extension (8 N·m) or flexion (8 N·m) bending moment are applied, close to physiological range (White and Panjabi, 1978). These are also shown on Fig. 3.3-3.

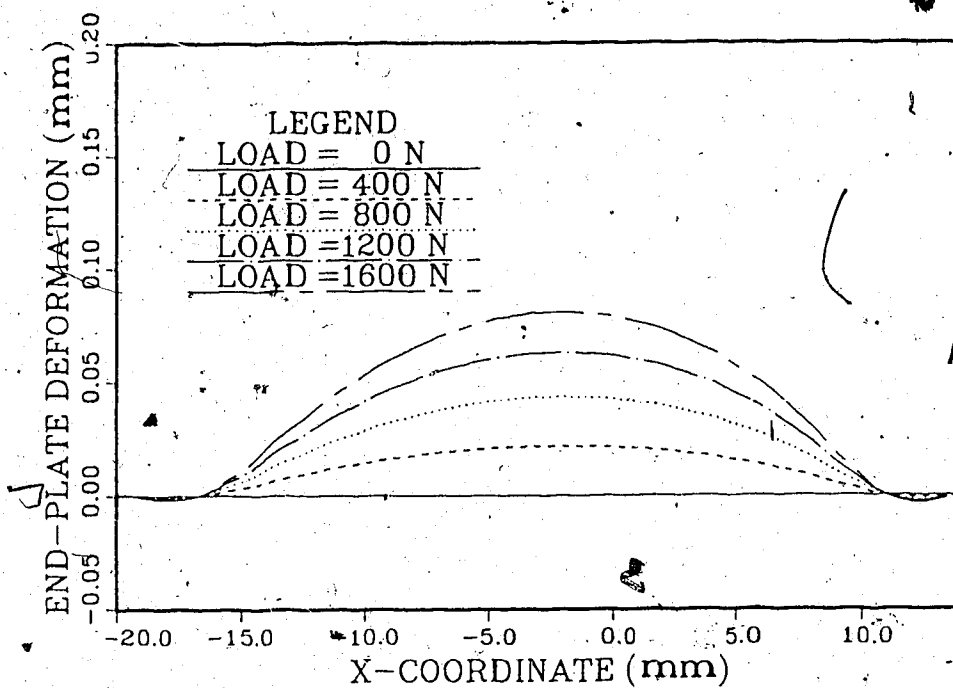


Figure 3.3-1: END-PLATE BULGING
(Under compression)

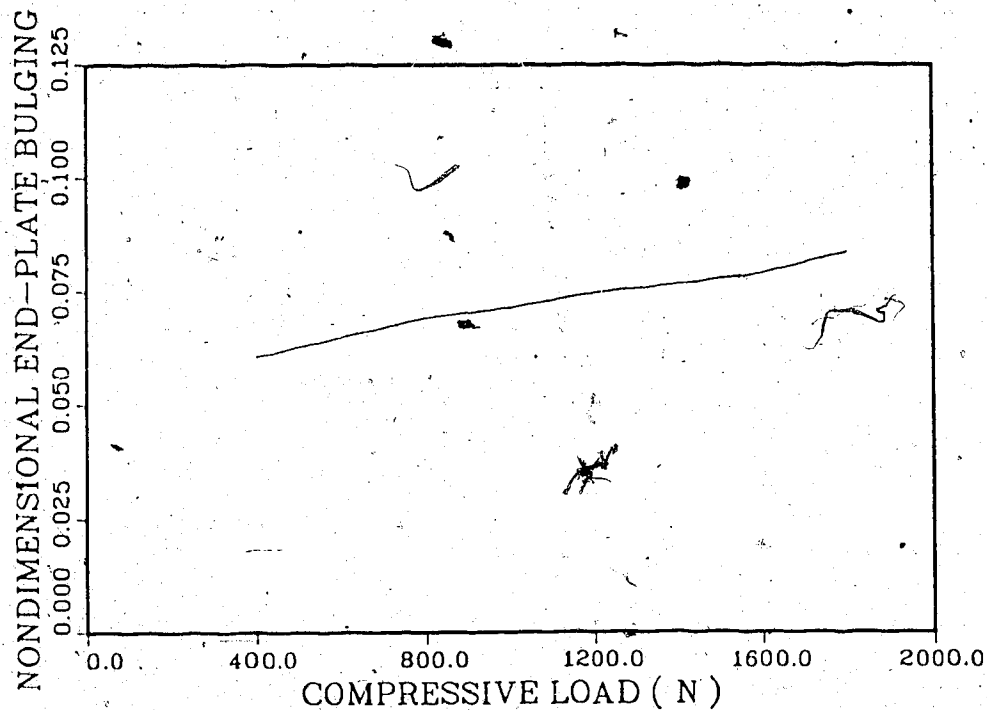


Figure 3.3-2: NONDIMENSIONAL END-PLATE BULGING PARAMETER

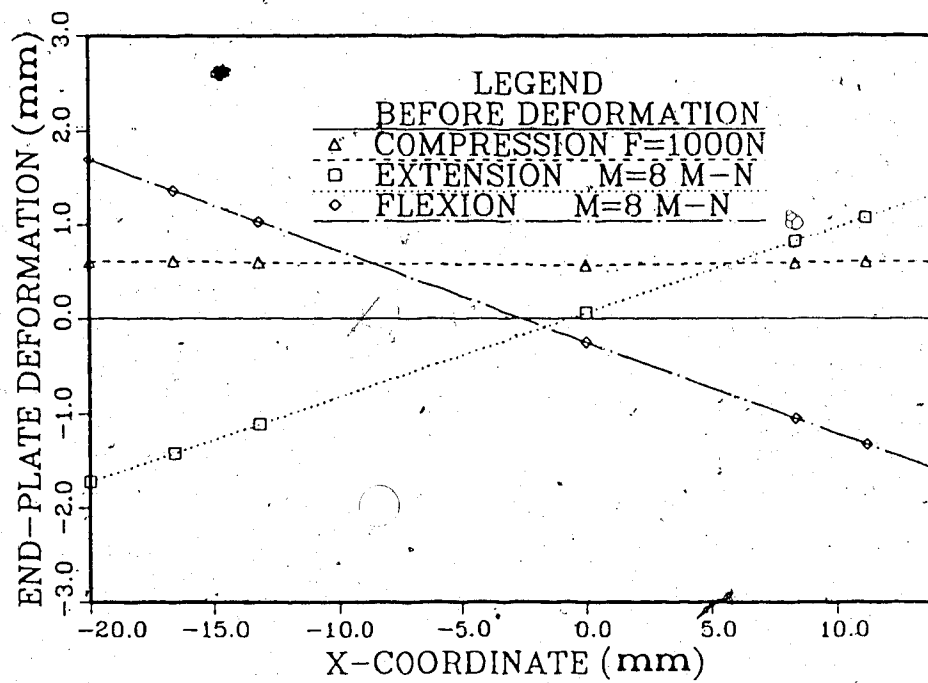


Figure 3.3-3: END-PLATE DEFORMATION UNDER
COMPRESSION, EXTENSION AND FLEXION

3-4: COLLAGENOUS FIBER STRAIN AND DISC BULGING

RELATED TO CLINICAL SYMPTOMS

Collagenous fiber strain and horizontal bulging of the intervertebral disc occur when spine motion segments are subjected to mechanical loads. Although the extent to which the intervertebral disc acts as a source of low-back pain is not clear, annulus rupture and disc bulging are known to relate to low-back pain (Jayson, 1976). Although not included in the objectives of this study, its results may contribute to understanding clinical symptoms mentioned above..

Fig. 3.4-1 shows a posterior view of the relationship of lumbar nerve roots to the vertebral body and the intervertebral disc. The spinal nerve roots leave the spinal cord and cross the posterolateral aspect of the disc to exit. If the annulus experiences a serious rupture, the disc may severely compress the nerve root (Fig. 3.4-2). This study can provide some information to explain reasons of posterior or posterolateral annulus rupture.

Fig. 3.4-3 and Fig. 3.4-4 illustrate the posterior and posterolateral collagenous fiber strain under different loading conditions. This study confirms that with daily physiological motion, corresponding to a compressive load of about 1000 N, the posterior and posterolateral collagenous fibers do not experience severe strain (about 1.5%). Based on this information, Farfan (1970) suggested that axial rotation may be the main reason for posterior annulus rupture. Fig. 3.4-3 and 3.4-4 indicate that axial rotation and flexion cause large strains in the posterior and posterolateral collagenous fibers. This suggests

Page 59 has been removed due to copyright restriction. This page
contained: POSTERIOR RELATIONSHIP OF LUMBAR NERVE ROOT

(From DePalma and Rothman, 1970)

and

A SEQUESTERED DISC MAY COMPRESS THE NERVE ROOT

(From DePalma and Rothman, 1970)

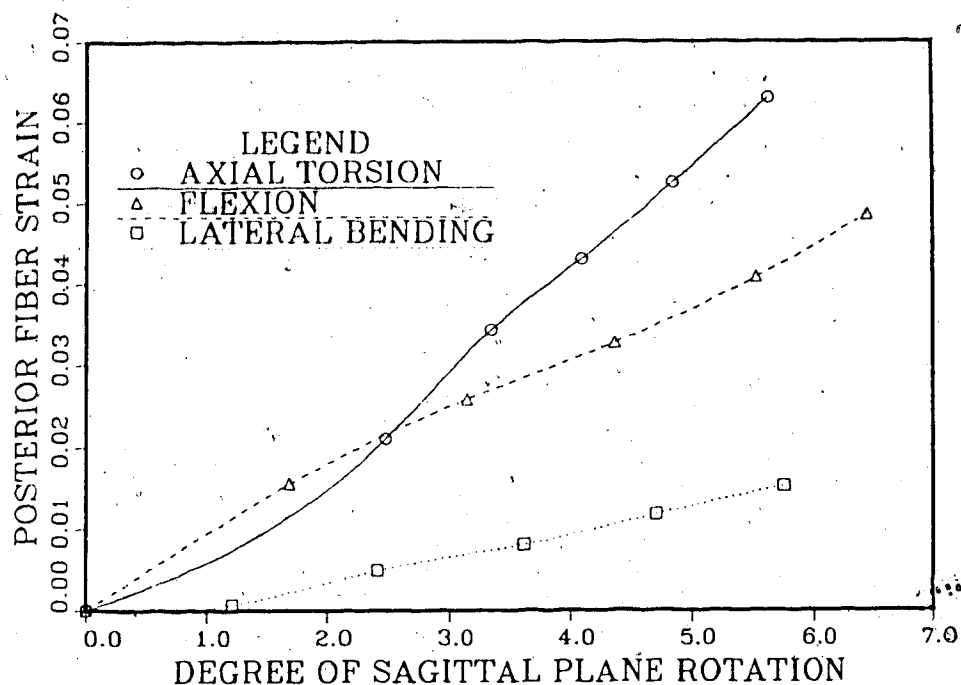


Figure 3.4-3: POSTERIOR COLLAGENOUS FIBER STRAIN
(Under different loadings)

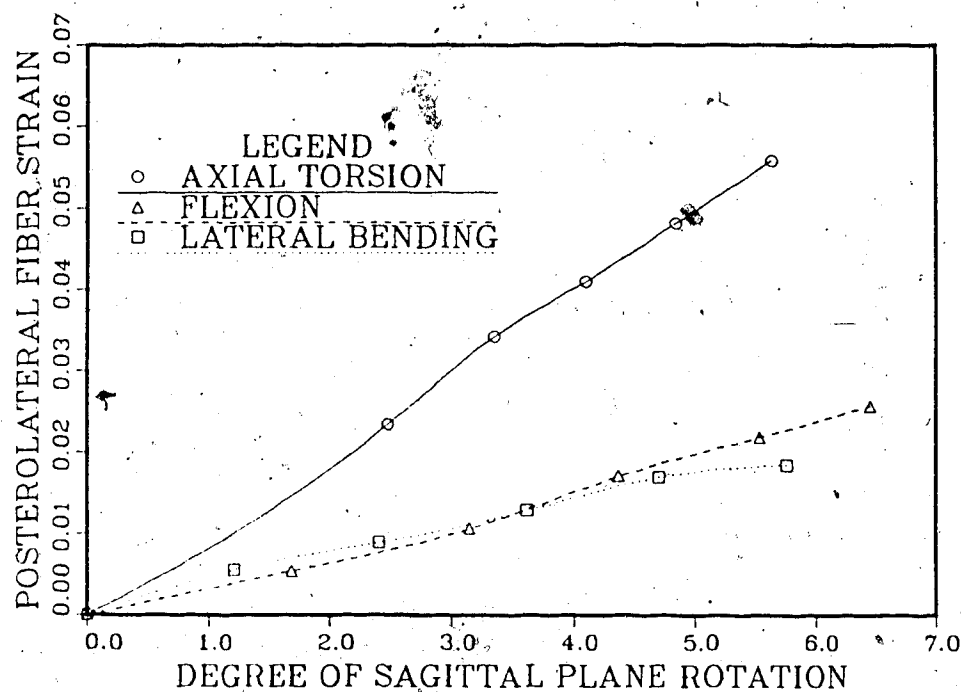


Figure 3.4-4: POSTEROLATERAL COLLAGENOUS FIBER STRAIN
(Under different loadings)

that axial rotation and flexion together may cause the posterior or posterolateral annulus failure.

This model also predicted that the posterior region experiences the largest horizontal bulging (Fig. 3.4-5).

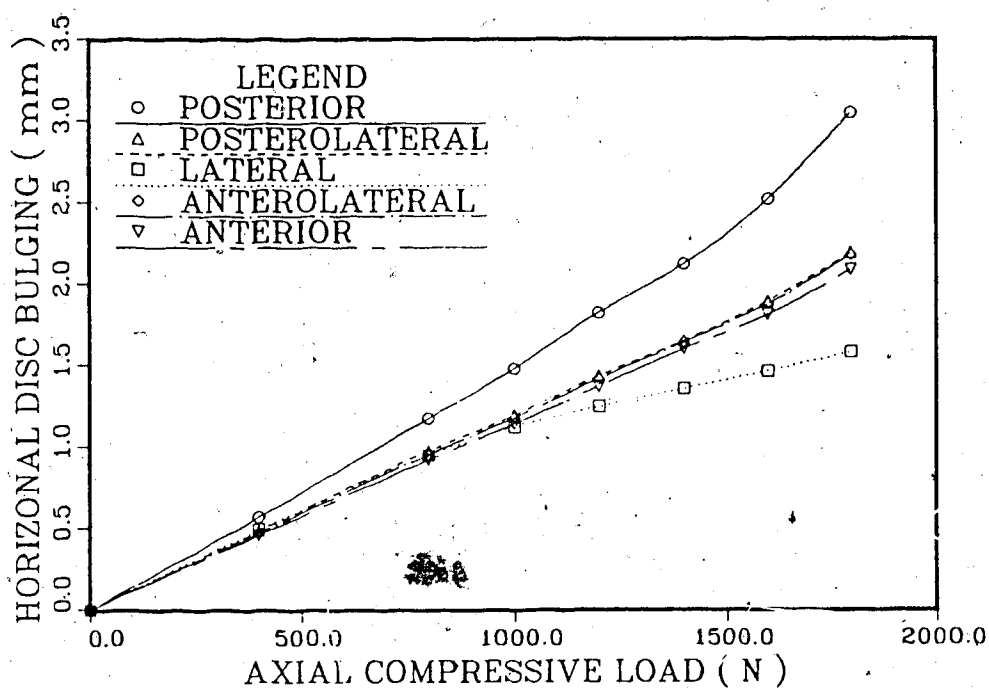


Figure 3.4-5: HORIZONTAL DISC BULGING
(Under compression)

3-5: GROSS DISC BEHAVIOUR UNDER SEPARATE LOADS

The gross disc behaviour with respect to extension, flexion, lateral bending and axial torsion are plotted in Fig. 3.5-1. Compared to flexion, extension and lateral bending, the disc response is more stiff with respect to axial torsion. All this information has an implication for simplifying the model of the intervertebral disc in spine fixation system. The disc can be replaced by multi-string systems which have different stiffnesses with respect to applied forces and torques. Its stiffnesses K_c (compression stiffness), K_e (extension stiffness), K_f (flexion stiffness), K_l (lateral bending stiffness) and K_r (rotation stiffness) can be piecewisely approximated from Fig. 3.5-1. These stiffness parameters can be used in constitutive relations when the disc is modeled in a simple manner. Such a simplified model of some discs could reduce the computational requirements for a model of the complete spine.

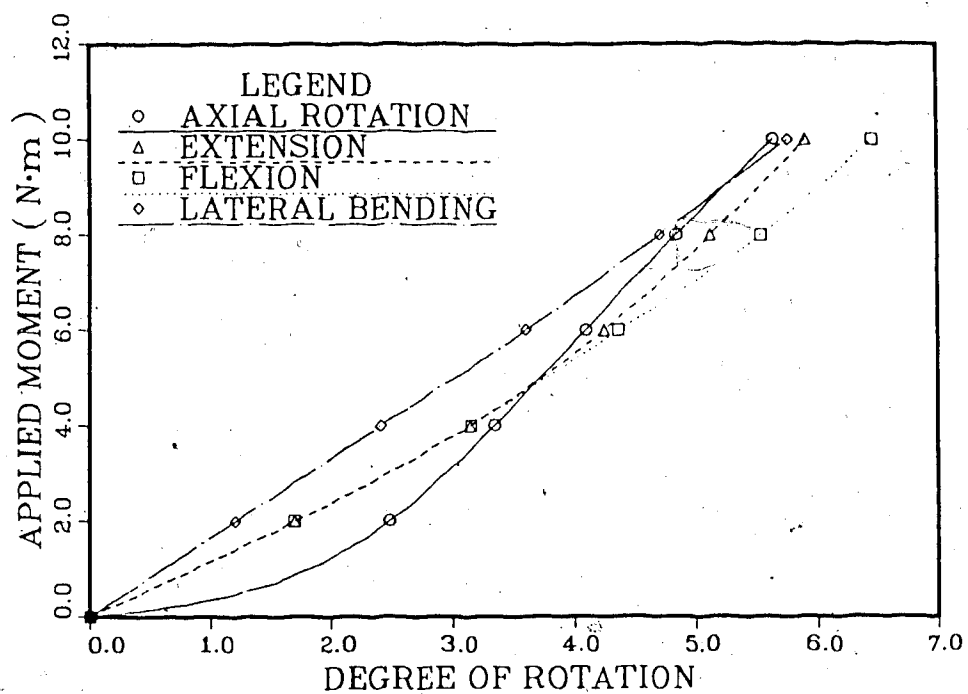


Figure 3.5-1: DISC SAGITTAL PLANE ROTATION
(Under flexion, extension, lateral bending and axial rotation)

CHAPTER 4: MODELING THE ANNULUS FIBROSUS

4-1: INTRODUCTION

In published literature, there are two ways of modeling the annulus fibrosus using the finite element method. Some investigators (Belychko et al, 1974; Kulak et al, 1976; Spilker et al, 1986) represented the annulus which is composed of collagenous fibers and ground substance by a composite material (composite model). Others (Ueno et al, 1982; Shirazi-Adl et al, 1984, 1986) used a cable element for the collagenous fiber and an elastic element for the ground substance. The ends of the cable element are embedded in the elastic element (fiber-reinforced model).

This study used the fiber-reinforced model, because of the lack of nonlinear composite material moduli in the published literature.

As mentioned in 1-8, a consideration in modeling the spine fixation system is the intradiscal boundary condition. The concern was whether different annulus models affect the normal stress distribution in the end-plate.

To compare two different models of the annulus fibrosus, the annulus fibrosus was modeled by 80 8-node 3-D orthotropic composite linear elastic elements. The composite model is geometrically identical with the fiber-reinforced model. The orthotropic material moduli were

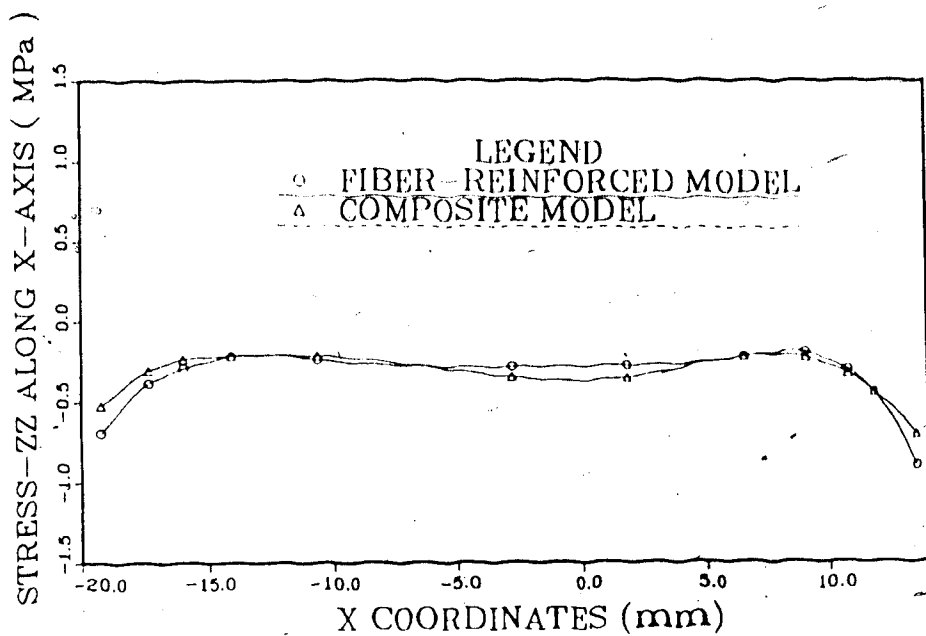
reported by Spilker et al (1986). Comparisons were made between these two models, especially their effects on the stress distributions in the end-plate.

4-2: STRESSES IN THE END-PLATE IN TWO DIFFERENT MODELS

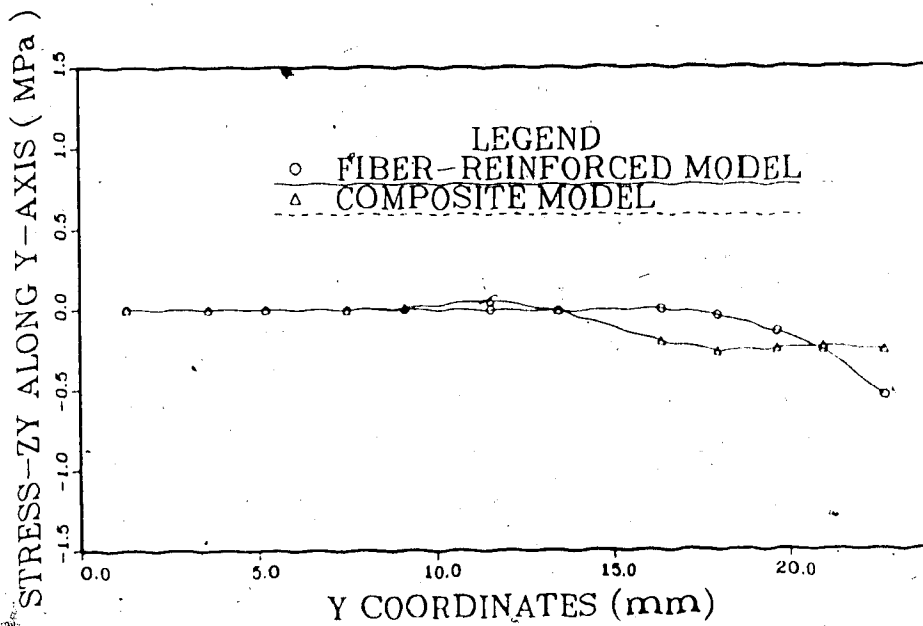
Fig. 4.2-1 shows that there are no great differences between the models for two models for the normal stress σ_{zz} distribution along the X-axis.

Fig. 4.2-2 shows the shear stress σ_{zx} distribution along the Y-axis. It is apparent that both models showed zero shear stress σ_{zx} in the central end-plate region, adjacent to the nucleus pulposus. The non-shear stress region in the end-plate of the fiber-reinforced model is larger than that of the composite model. This implies that for the fiber-reinforced model, the vertebra restriction to the horizontal bulging of the annulus is achieved primarily by the outside fibers of the annulus which are attached to the end-plate. However for the composite model, this restriction exists uniformly through the thickness of the annulus. The highest value of shear stress σ_{zx} of the fiber-reinforced model is about double that for the composite model.

Another difference between the two models is the stress distribution in the annulus. Subjecting the fiber-reinforced model to a compressive load causes tension in the fibers and triaxial compression in the ground substance. The annulus fibrosus experiences circumferential tension in the composite model, because the annulus fibrosus is represented as a uniform material.

FIG. 4.2-1: NORMAL STRESS σ_{zz} DISTRIBUTION

(With two different models)

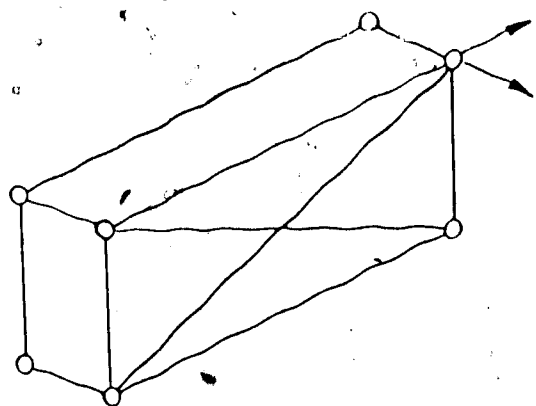
FIG. 4.2-2: SHEAR STRESS σ_{zy} DISTRIBUTION

(With two different models)

4-3: MODELING THE SLIDING BETWEEN THE COLLAGENOUS FIBERS AND THE GROUND SUBSTANCE

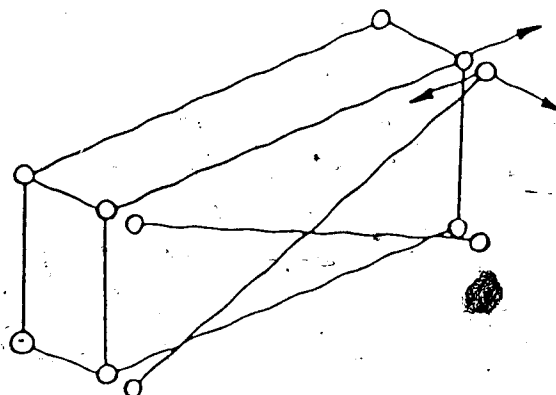
As mentioned in 1-3, one of the basic functions of the ground substance is to lubricate (Frankel and Nordin, 1980) the collagenous fibers. Other investigators (Spilker et al, 1986) also stated the necessity of accounting for the interaction between the collagenous fibers and the ground substances. In this fiber-reinforced disc model, the ends of collagenous cable elements are embedded in 3-D elastic elements representing the ground substance. At each node, the collagenous fiber and the ground substance are fixed together (Fig. 4.3-1). Physically this means that the fiber-reinforced model (Ueno et al, 1983; Shirazi-Adl et al, 1984, 1986) can not account for ground substance lubrication.

Using the fiber-reinforced model, sliding between the collagenous and the ground substance can be accommodated by specifying two nodes at the interface; one node for the collagenous fiber and another for the ground substance. For each pair of nodes, a local coordinate system is set up so that one axis is the tangent to the sliding interface and the other is normal to the sliding interface. In the normal direction, the two node points will have the same motion, however in the direction of the tangent the nodes will have separate motion, thus enabling the two materials to slide on each other (Fig. 4.3-2).



Two nodes move together

FIG. 4.3-1: COLLAGENOUS FIBER ELEMENTS AND
GROUND SUBSTANCE ELEMENT FIXED TOGETHER



Two nodes allowed to
slide on each other

FIG. 4.3-2: TWO KINDS OF ELEMENTS ALLOWED TO SLIDE ON EACH OTHER

4.4. MODELING THE ANNULUS FIBROSUS

Anatomically the collagenous fibers are inclined with respect to the horizontal plane. The angle of inclination changes alternatively from one band to the next. The range of variation of this angle is from 24° to 45° , with an average of 30° (White and Panjabi, 1978; Horton 1958). Since the ground substance is relatively soft, the deformation behaviour of the annulus in tension is dependent directly on the collagenous fibers.

When the disc is subjected to compressive load, Shah et al (1970) experimentally found maximum tangential strain of the annulus occurred at the posterolateral surface. Based on this information, it can be estimated that posterior or posterolateral collagenous fibers experience the maximum tension strain. This result was not obtained by the fiber-reinforced model. It was found that the specified alignment of collagenous fiber significantly affects the collagenous strain distribution in different locations. For example, when the inclination of the posterolateral fiber decreases from 30° to 27.5° , strain increases 54% from 0.0109 to 0.0168, under compressive displacement load 1.0 mm. Although Shirazi-Adl et al (1984) computed that the collagenous fibers of all layers undergo tensile strains when the disc is subjected to compression, they found minimum strains at the out layers, increasing towards the inner layers. However, they did not state the locations, for posterior or other regions, of the maximum strains.

The greatest discrepancy among the different investigators involves

the prediction of annulus strain. Therefore a more physiological model of the annulus is needed.

CHAPTER 5: DISCUSSION AND CONCLUSION

5-1: Material Properties

As mentioned in 1.4, both cortical and cancellous bone are anisotropic material but a lack of published data on the anisotropic material properties required the use of isotropic elastic elements in the model. This was done primarily to simplify the finite element model without sacrificing the overall effects of these parts on the segment behaviour. In view of the small strains experienced by the bony elements and the negligible ratios of the final stresses to the moduli, other constitutive relations are not expected to make any noticeable difference in the predictions. The annulus ground substance undergoes large strains reaching stresses which are of the same order of magnitude as its moduli. However, because of a lack of published data on the material properties of the annulus ground substance, it was assumed to obey a constitutive relation independent of the state of stress.

5-2: STRESSES ON THE END-PLATE AND END-PLATE BULGING

Although measurements have been done on nucleus pressure (Nachemson, 1960, 1981), mechanical properties of the annulus fibrosus (Galante, 1967; Wu and Yao, 1976), and annulus fibrosus strains (Shah et al, 1978), little work has been done on the stress state of the end-plate. Theoretical models of the loaded body-disc unit are supported only in one point by experimental stress data: Nachemson's measurement of the pressure in the nucleus pulposus. A complete stress analysis of the body-disc unit requires knowledge of the three normal stress and shear stress components for each volume element. It is unlikely that it will be possible to measure all these six stress components simultaneously. Horst and Brinckmann (1981) measured the normal stress distribution on the end-plate of the vertebral body by the aid of miniature piezoelectric pressure transducers. To the author's knowledge, this is the only report on experimental measurement of stresses on the end-plate. Therefore they become the only basis to support predictions in this thesis. As mentioned in 3-2, compressive load causes normal stress that are uniformly distributed on the central end-plate region, adjacent to the nucleus pulposus. In the peripheral end-plate region, the normal stress σ_{zz} becomes greater, starting from the interface between the nucleus and the annulus, and remain uniform throughout the outer region of the end-plate. This is contrary to that of Horst and Brinckmann. They found the normal stress σ_{zz} distributed uniformly throughout the whole cross-section of the end-plate. In Horst and Brinckmann's experiment, only five pressure transducers were used to

sample the stress distribution simultaneously on the end-plate. The transducers had a sensitive area of 6 mm in diameter (the sagittal diameter of the present model is 34 mm). As well, equipment set-up may have affected the accuracy of measurements. More experimental work is required to detail the stress distribution on the end-plate.

5-3: LIMITATIONS OF THIS STUDY

The motion segment model in this study did not include posterior elements, ligaments and muscles. "In vitro" measurements on intact lumbar motion segment have shown that even under pure axial compression, 18% of the load is transmitted through the articular facets (Nachemson, 1960). If this is true "in vivo", then the present analysis must be considered an approximation. This was not unexpected since this study was intended to be a first step in the development of a more sophisticated model.

This study did not take into account the rate-dependent response behaviour of the disc-body unit. Therefore the predictions of stresses and strains in the unit can be interpreted only in terms of those external loading conditions for which the assumptions of static or quasi-static analysis are justified. This limitation excludes consideration of such dynamic situations as vibration and impact.

It must be emphasized that the present analysis is concerned with the response of the lumbar motion segment only under pure compression, flexion, extension, lateral bending and axial rotation. In life, the motion segment seldom experiences only one kind of load.

5-4: CONCLUSIONS

A three-dimensional finite element program was used to analyze a model of the lumbar disc-body unit. The program included both geometric and material nonlinearities. The annulus fibrosus was modeled as a composite with collagenous fibers embedded in a matrix of ground substance. The nucleus pulposus was represented by an inviscid incompressible fluid. Pure compression load, flexion, extension, lateral bending and axial torsion loads were applied to the disc-body unit.

Validation of the model by a comparison of its predictions with reported results of "in vitro" measurements indicate good agreement. This study predicted the existence of large strains and deformations in the unit even under moderate loads, so that large strain and deformation analysis is required.

This study concludes the following:

- (1) The disc-body unit exhibits a stiffening behaviour with increasing loads. The bony elements experience low stresses (below 1% of their elastic moduli) compared to the intervertebral disc (about 100% of their elastic moduli).
- (2) The end-plate deformed as a rigid body compared with the large deformation experienced by the intervertebral disc. This rigidity exists in all loading cases.
- (3) In general, the stresses are uniformly distributed on the central end-plate region, starting from the interface between the

nucleus and the annulus, stresses change to a greater magnitude and stay nearly uniform on the periphery of the end-plate.

(4) There exist a non-shear stress area on central end-plate region, adjacent to the nucleus pulposus.

(5) The intradiscal boundary conditions can be modeled as either displacement or force boundary conditions. The rigid surface can be specified on either top or bottom of spine fixation systems.

Based on the stress distribution on the end-plate, loads can be applied in similar manner.

Further development of this model and some suggestions are included as following:

(1) Better representation of collagenous fiber inclination angle is needed. This can be done through X-ray examination of cadaver specimen. The annulus model can be identical to experimental results.

(2) Posterior elements need to be attached to the model. Three-dimensional digitizing system can be used to obtain detailed geometry of posterior elements. Ligaments and deep muscles are also need to be included. After this, posterior joint interaction can be studied.

- (3) In a spine fixation model, vertebrae can be modeled as rigid bodies in non-critical regions. Intervertebral discs can be replaced by multi-strings in spine fixation systems where their gross stiffnesses can be piecewise approximated from results on this study.
- (4) In fractured vertebra, special distorted high-order isoparametric elements (Henshell and Shaw, 1975; Barsoum, 1976) can be employed at a crack tip. This kind of element contains stress singularities and enable to investigate detailed motion behaviour around the crack tip.
- (5) Representation of different fixation techniques and their action on spine should be studied as well.

After all these studies, the model can be extended to time dependent behaviour study such as dynamic and relaxation etc.. Effective fixation techniques can be evaluated by a suitable finite element model.

REFERENCES

- 1: Abrahams M. (1967): Mechanical behavior of Tendon in vitro: a preliminary report. Med. Biol. Eng. 5: 433-443.
- 2: ADINA Users Manual (1981).
- 3: ADINA-PLOT Users Manual (1983).
- 4: ADINA System Theory and Modeling Guide (1984).
- 5: Barsoum R.S. (1977): Triangular quarter-point element on elastic and perfectly plastic crack tip elements. Int. J. Num. Mech. Eng. 11: 85-98.
- 6: Bathe K.J. (1982): Finite Element Procedures in Engineering Analysis. New Jersey, Prentice-Hall, Englewood Cliffs.
- 7: Bathe K.J. and Hahn W.F. (1979): On the transient analysis of fluid-structure systems. Computers & Structures 10: 383-391.
- 8: Belytschko T.B., Kulak R.F., Schultz A.B. and Salante J.D. (1974): Finite element stress analysis of an intervertebral disc. J. Biomechanics 7: 277-285.
- 9: Brickley Parsons D. and Glimcher M.J. (1984): Is the chemistry of collagenous in intervertebral discs an expression of Wolff's law? Spine 9: 148-163.
- 10: Broberg K.B. and Von H.O. Esson (1980): Modeling of intervertebral discs. Spine 5: 155-167.
- 11: Broberg K.B. (1983): On the mechanical behavior of intervertebral discs. Spine 8: 151-165.

- 12: Brown N., Saputa C. and Black J. (1981): Young's modulus of living human bone. Transactions of the 27th Annual Meeting, Orthop Res. Soc. 6: 41.
- 13: Burstein A.H., Reilly D.T. and Martens M. (1976): Aging of bone tissue: Mechanical properties. J. Bone Joint Surg. 58A: 82-86.
- 14: Cairney J. and Cairney John (1974): The Human Body. N.M. Peryer Limited.
- 15: Carlstedt C.A. (1986): A model for computer-aided analysis of biomechanical properties of the plantaris longus tendon in the rabbit. Biomechanics 19: 251-256.
- 16: Carter D.R. and Hayes W.C. (1976): Bone compressive strength: The influence of density and strain rate. Science 194: 1174.
- 17: Carter D.R. and Hayes W.C. (1977): The compressive behavior of bone as a two-phase porous structure. J. Bone Joint Surg. 59A: 954.
- 18: Cossette J.W., Farfan H.F., Robertson G.H. and Wells R.V. (1971): The instantaneous center of rotation of the third lumbar intervertebral joint. J. Biomechanics 4: 149-153.
- 19: Cowin S.C. (1983): On the composite material modeling of bone, Mechanics of Composite Materials. Edited by Dvorak G.J..
- 20: Crouch J.E. (1982): Essential Human Anatomy. Philadelphia, Lea & Febiger.
- 21: DePalma and Rothman (1970): The Intervertebral Disc. W.B. Saunders Company.
- 22: Evans F.G. (1973): Mechanical Properties of Bone. Illinois, C.C. Thomas, Springfield.

- 23:Farfan H.F. (1969): Effects of torsion on the intervertebral joint.
Can. J. Surg. 12: 336-341.
- 24:Farfan H.F., Cossette J.W., Robertson G.H., Wells R.V. and Kraus H.
(1970): The effects of torsion on the lumbar intervertebral
joints: The role of torsion in the production of disc
degeneration. J. Bone Joint Surg. 52A: 468-497.
- 25:Farfan H.F. (1973): Mechanical Disorder of the Low Back.
Philadelphia, Lea &Febiger.
- 26:Frankel V.H. and Burstein A.H. (1970): Orthopaedic Biomechanics.
philadelphia, Lea & Febiger.
- 27:Frankel V.H. and Nordin M. (1980): Basic Biomechanics of the Skeletal
System. Philadephia, Lea & Febiger.
- 28:Galante J.O. (1967): Tensile properties of the human lumbar annulus
fibrosus. Acta orthop. scand. (Suppl.) 100: 1-90.
- 29:Grant J.C. (1972): An Atlas of Anatomy. Williams & Wilkins.
- 30:Hakim N.S. and King A.I. (1979): A three dimensional finite element
dynamic response analysis of vertebra with experimental
verification. J. Biomechanics 12: 277-292.
- 31:Harkness R.D. (1961): Biological functions of collagen. Biol. Rev.
36: 399-463.
- 32:Haut R.C. and Little R.W. (1972): A constitutive equation for
collagen fibres. J. Biomechanics 5: 423-430.
- 33:Henshell R.D. and Shaw K.C. (1972): Finite elements are
unnecessary, Int. J. Num. Mech. -Eng. 9: 495-507.
- 34:Hickey D.S. and Hukin D.W.L. (1980): Relation between the structure

- of the annulus fibrosus and the tension and failure of intervertebral disc. Spine 5: 16.
- 35: Horst M. and Brinckmann D. (1977): Measurement of the distribution of axial stress on the end-plate of the vertebral body. Spine 6: 217-232.
- 36: Horton W.G. (1958): Further observations on the elastic mechanism of the intervertebral disc. J. Bone Joint Surg. 40B: 552-557.
- 37: Jayson M. (1976): The Lumbar Spine and Back Pain. New York, San Francisco, Grune & Stratton.
- 38: Kulak R.F., Beltschko T.B., Schultz A.B. and Galante J.O. (1976): Non-linear behavior of the human intervertebral disc under axial load. J. Biomechanics 9: 377-386.
- 39: Lin H.S., Liu Y.K., Ray G. and Nikravesh P. (1978): System identification of material properties of the intervertebral joint. J. Biomechanics 11: 1-14.
- 40: Lindahl D. (1975): Mechanical properties of dried defatted spongy bone. Acta Orthop. Scand. 47: 11-19.
- 41: Markolf K.L. (1972): Deformation of the thoracolumbar intervertebral joints in response to external loads. J. Bone Joint Surg. 54A: 511-533.
- 42: Markolf K.L. and Morris, J.M. (1974): The structural components of the intervertebral disc: a study of their contributions to the ability of the disc to withstand compressive forces. J. Bone Joint Surg. 56A: 675-687.
- 43: McAfee P.C., Werner F.W. and Glisson R.R. (1985): A biomechanical

analysis of spinal instrumentation systems in thoracolumbar fractures. Spine 10: 204-217.

44:McFarland W.N., Pough F.H., Cade T.J. and Heiser J.B. (1979):

Vertebrate Life. Macmillan Co. Inc..

45:Nachemson A.L. (1960): A lumbar intradiscal pressure. Acta. orthop. scand. (Suppl.)43: 1-104.

46:Nachemson A.L. (1981): Disc pressure measurements. Spine 6: 93-97.

47:Ranu H.S., Denton, R.A. and King, A.I. (1979): Pressure distribution under an intervertebral disc - an experimental study. J. Biomechanics 12: 807-812.

48:Reuber M., Schultz A.B., Denis F., Spencer. D.: Bulging of lumbar intervertebral disc. J. Biomech. Eng. 104: 187-192.

49:Rolander S.D. (1966): Motion of the lumbar spine with special reference to the stabilizing effect of posterior fusion. Acta. Orthop. Scand. (Suppl.) 90: 1-144.

50:Rolander S.D. and Blair W.E. (1975): Deformation and fracture of the lumbar vertebral end-plate. Orthop. Clin. North. Ameri. 6: 75-81.

51:Sanjeevi R. (1982): A viscoelastic model for the mechanical properties of biological materials. J. Biomechanics 15: 107-109.

52:Sanjeevi R., Somannathani N and Ramaswamy D. (1982): A viscoelastic model for collagenous fibers. J. Biomechanics 15: 181-183.

53:Schureiner K.E. (1983): Fiber stabilization of bent cylinders, with an application to intervertebral disks. J. Biomech. Eng. 105: 294-295.

✓ 54:Schultz A.B., Warwick D.N., Berkson, M.H., Nachemson A.L. (1979): Mechanical properties of human lumbar spine motion segments I:

- Responses in flexion, extension, lateral bending, and torsion. J. Biomech. Eng. 101: 46-52.
- 55: Shah J.S., Hampson W.G.J. and Jayson M.I.V. (1978): The distribution of surface strain in the cadaveric lumbar spine. J. Bone Joint Surg. 60B: 246-251.
- 56: Shirazi-Adl A., Ahmed A.M. and Shrivastava S.C. (1984): Stress analysis of the lumbar disc-body unit in compression: A three-dimensional nonlinear finite element study. Spine 9: 120-134.
- 57: Shirazi-Adl A., Ahmed A.M. and Shrivastava S.C. (1986): A finite element study of a lumbar motion segment subjected to pure sagittal plane moments. J. Biomechanics 19: 331-350.
- 58: Shirazi-Adl A., Ahmed A.M. and Shrivastava S.C. (1986): Mechanical response of a lumbar motion segment in axial torque alone and combined with compression. Spine 11: 914-927.
- 59: Simon B.R., Wu J.S., Carlton M.W., Kazarian L.E., France E.P., Evans J.H. and Zienkiewicz (1985): Poroelastic dynamic structural models of rhesus spinal motion segments. Spine 10: 494-506.
- 60: Sonnerup L. (1972): A semi-experimental stress analysis of the human intervertebral disc in compression. Exp. Mech. 12: 142-147.
- 61: Spilker R.L. (1980): A simplified finite element model of the intervertebral disc. Finite Elements in Biomechanics. Edited by B.R. Simon, Tuscon, University of Arizona.
- 62: Spilker R.L., Daigirda D.M. and Schultz A.B. (1984): Mechanical response of a simple finite element model of the intervertebral disc under complex loading. J. Biomechanics 17: 103-112.

- 63:Spilker R.L., Jakobs D.M. and Schultz (1986): Material constants for a finite element model of the intervertebral disc with a fiber composite annulus. J. Biomech. Eng. 108: 1-11.
- 64:Sundqvist Jan (1983): An application of ADINA to the solution of fluid-structure interaction problems. Computers & Structures 17: 793-807.
- 65:Ueno K., Liu Y.K. and Chandran K.B. (1982): A three-dimensional finite element model of the L4-L5 intervertebral joint. Annual Meeting of the intervertebral Society for the Study of the Lumbar Spine, Toronto.
- 66:Ueno K. and Liu Y.K. (1985): A three-dimensional nonlinear finite element model of lumbar intervertebral joint in torsion. 1985 Biomechanics Symposium, ASME: 97-100.
- 67:Tencer A.F., Ahmed A.M. and Burke D.L. (1981): The role of secondary variables in the measurement of the mechanical properties of the lumbar intervertebral joint. J. Biomech. Eng. 103: 129-137.
- 68:Virgin W.J. (1951) Experimental investigations into the physical properties of the intervertebral disc. J. Bone Joint Surg. 33B: 607-611.
- 69:Weaver J.K., Chalmers J. (1966): Cancellous bone: its strength and changes with aging and an evaluation of some methods for measuring its mineral content. J. Bone Joint Surg. 48A: 289-308.
- 70:White A.A.III and Panjabi M.M. (1978): Clinical Biomechanics of the Spine. Philadelphia and Toronto, J.B. Lippincott.
- 71:Wu H.C. and Yao R.F. (1976): Mechanical behavior of the human annulus fibrosus. J. Biomechanics 9: 1-7.

72:Yamada H. (1970): Strength of Biological Materials. Edited by F.G. Evans, Baltimore, Williams & Wilkins.

73:Yang K.H. and King A.I. (1984): Mechanism of facet load transmission as a hypothesis for low back pain. Spine 9: 557-565.

APPENDIX A: INTRODUCTION OF ADINA

This appendix introduces the use of the finite element computer program ADINA (Automatic Dynamic Incremental Nonlinear Analysis). ADINA is a computer program for the static and dynamic displacement and stress analysis of structures and fluid-structure systems. The program can be employed to perform linear and nonlinear analysis. The program has been designed to perform a linear analysis very effectively. Following a linear analysis, a nonlinear analysis can then be carried out with relatively few data input changes.

The program ADINA is the main module of the ADINA system. The complete ADINA system consists currently of the program ADINA for displacement and stress analysis, ADINAT for analysis of heat transfer and field problems, ADINA-IN for preparation and display of the input data and ADINA-PLOT for display of the calculated solution results. The objective in this introduction is to briefly overview the current use of ADINA.

Incremental Equilibrium Equations:

The basic equations that ADINA used in this nonlinear elastic static analysis are:

$$\begin{bmatrix} {}^t K_L & {}^t K_{NL} \end{bmatrix} \Delta U^{(i)} = {}^{t+\Delta t} R - {}^{t+\Delta t} F^{(i-1)} \quad [1]$$

The terms in equ. [1] are:

${}^t_{tL} K$, ${}^t_{tNL} K$: linear, nonlinear stiffness matrix in the configuration at time t .

ΔU : vector of incremental nodal point displacements.

${}^{t+\Delta t} R$: vector of external loads at time $t+\Delta t$.

${}^{t+\Delta t}_{t+\Delta t} F$: vector of nodal point forces at time $t+\Delta t$.

and the superscript (i) indicates "i"th iteration.

Solution of Equations:

Of much concern is the stability and accuracy of the incremental solution of nonlinear equations. In ADINA the solution of equ. [1] can be obtained using the modified or full Newton-Rapson methods with or without line searches, The BFGS method (ADINA Users Manual). This study employs the BFGS method (Bathé, 1982), the algorithm used is

$${}^t_{K^*} \Delta U^{(i)} = {}^{t+\Delta t}_{t+\Delta t} R - {}^{t+\Delta t}_{t+\Delta t} F^{(i-1)} \quad [2]$$

$${}^{t+\Delta t}_{U(i)} = {}^{t+\Delta t}_{U(i-1)} + \beta \Delta U^{(i)} \quad [3]$$

where ${}^t_{K^*}$ is an updated stiffness (linear and nonlinear) matrix (based on the iteration history) and β is an accelerating factor determined by a line search in the direction of $\Delta U^{(i)}$.

The convergence criteria for successful iteration are satisfied when both

$$\frac{\| \begin{pmatrix} t+\Delta t \\ R \end{pmatrix} - \begin{pmatrix} t+\Delta t \\ F(i-1) \end{pmatrix} \|_2}{RNORM} \leq RTOL \quad [4]$$

$$\frac{\Delta U(i) \left(\begin{pmatrix} t+\Delta t \\ R \end{pmatrix} - \begin{pmatrix} t+\Delta t \\ F(i-1) \end{pmatrix} \right)}{\Delta U(i)^T \left(\begin{pmatrix} t+\Delta t \\ R \end{pmatrix} - \begin{pmatrix} t \\ F \end{pmatrix} \right)} \leq ETOL \quad [5]$$

where $\| F \|_2$ denotes the Euclidean norm of vector F , hence

$\| F \|_2 = (F_1^2 + F_2^2 + \dots + F_n^2)^{1/2}$ in equ. [4]; ETOL is defined

by $ETOL = 10 \times DTOL \times RTOL$, where DTOL is are relative displacement tolerance and RTOL is relative force tolerance. Thus equ. [5] embodies the displacement convergence check. In this study, DTOL and RTOL are specified as 0.01 and 0.1 respectively through the input data file.

Constraint Equations:

In this study, it is necessary to prescribe displacement at some nodal points, and/or impose constraints between some nodal displacement components. In ADINA the following relationships can be specified

$$U_i = f_i(t) \quad [6]$$

and

$$U_k = \sum_j \beta_j U_j \quad [7]$$

where $f_i(t)$ is a general time function (input to ADINA) that prescribes the nodal displacement U_i . The constraints in equ. [3] are specified as rigid links, in which case the program establishes the constraint equations automatically.

Load Definition.

Prescribed concentrated and pressure loads are defined. The prescribed displacement is also employed in this study.

Element Library and Material Models.

The program ADINA contains a unique and effective elements which can be used to model a large variety of problems. Element library and material models are summarized as following (ADINA System Theory and Modeling Guide, 1984):

Element Library:

Truss and cable elements

Two-dimensional solid elements.

Three-dimensional solid elements

Beam element.

Isoparametric beam elements

Plate/shell element

Shell elements

Pipe element

General elements

Two- and three-dimensional fluid elements.

Material Models:

Linear elastic models

Thermo-elastic model

Curve description model

Concrete model

Isothermal plasticity models

Thermo-elasto-plasticity and creep models

Rubber elasticity model

Truss nonlinear elastic model

User-supplied model.

The nonlinear elastic truss elements, 3-D elastic elements and 3-D fluid element are used for this analysis of fluid-structure interaction.

In the 3-D elastic element, two-point integration is employed.

For the truss element, the stress-strain relationship is defined as piecewise linear. The stress is uniquely defined as function of the strain only; hence for a specific strain, which is reached in loading or unloading, a unique stress is obtained by entering the stress-strain curve. One-point integration is used for the truss element according to the assumption that force is constant in the two-node truss.

Simply stated, the 3-D fluid element can be thought of as derived from the solid 3-D element by using an elastic stress-strain relation with a bulk modulus t_α and a zero shear modulus. The pressure is evaluated using the following relation:

$$t_p = t_\alpha \frac{\Delta V}{V_0} \quad [8]$$

where $\Delta V/V_0$ is the volumetric strain.

Using one-point integration order in fluid element,

constant pressure in each element, fulfills the principle that fluid is incompressible.

Supporting Literature on the ADINA System:

For the ADINA system the following documentation is available:

Users manuals gives the users manuals of the ADINA, ADINAT, ADINA-IN and ADINA-PLOT programs.

Theory and Modeling Guide describes the theory in ADINA and ADINAT computer programs. It also provide a bridge between the practical application of ADINA system and the detailed documentation of the theory. The report provides a compact description of the methods and assumptions used and gives in-detail references for further study.

The Verification Manual is meant to help the user in studies of the capabilities of the ADINA system, while at the same time it is used to verify the installation of the program on a specific computer. The description, solution and data input for a large number of problems are given in the manual.